PERFORMANCE INVESTIGATION OF DIFFERENT HYDROKINETIC TURBINES UNDER DIFFERENT SITE CONDITION

A DISSERTATION

Submitted in partial fulfillment of the
Requirement of award of degree
of
MASTER OF TECHNOLOGY
in
ALTERNATE HYDRO ENERGY SYSTEMS

By

RAJIV KUMAR TRIPATHI

DEPARTMENT OF HYDRO AND RENEWABLE ENERGY
INDIAN INSTITUTE OF TECHNOLOGY ROORKEE
ROORKEE-247667 (INDIA)
JUNE 2019

DECLARATION

I hereby declare that the report which is being presented here as the dissertation report on the topic "**PERFORMANCE INVESTIGATION OF DIFFERENT HYDROKINETIC TURBINES UNDER DIFFERENT SITE CONDITION**" in partial fulfillment of the requirements for the award of the degree of **Master of Technology** in **Alternate Hydro Energy Systems**, submitted in Department of Hydro and Renewable Energy, Indian Institute of Technology Roorkee, Uttarakhand, India, is an authentic record of my own work carried out under the supervision of **Dr. R. P. SAINI**, Professor, Department of Hydro and Renewable Energy, Indian Institute of Technology Roorkee.

I have not submitted the matter embodied in this report for the award of any other degree or diploma.

Date: June, 2019

Place: Roorkee **RAJIV KUMAR TRIPATHI**

CERTIFICATE

This is to certify that the above statement made by the candidate is correct to the best of my knowledge.

Dr. R. P. Saini
Professor
Department of Hydro and Renewable Energy
Indian Institute of Technology
Roorkee -247667

ABSTRACT

Energy crisis and the consumption of conventional energy resources have paid a great attention towards the use of renewable energy. The conventional energy sources are depleting day by day. The alternate energy resources are hence required. This is where the renewable source of energy comes into picture. The growth of civilization has been linked to our ability to capture and use the force of flowing water to our benefit. As lot of potential is available in flowing streams, so natural power available in streams has gained keen interest in electricity production for many years. Energy of waterways is mainly extracted by means of conventional hydropower plants that require some kind of a dam or reservoir. In the past, hydropower has been seen as a viable resource apparently to have little effect on the environment as river flow modifications and temperatures cause adverse effects to fish and other marine life. Therefore, the tidal energy systems were adapted for river energy extraction, which have their origins in wind energy extraction technologies.

Hydrokinetic energy is one of the most emerging technologies for power generation, it has gained keen interest of the researchers because of unique properties of water such as higher specific weight, higher momentum than air for same velocity and conditions. Hydrokinetic energy can be deployed in run of rivers, streams or waterways, where sufficient potential in the form of kinetic energy is available.

Under present dissertation work analytical and numerical investigation of different hydrokinetic turbines have been carried out through literature survey and factors on which site conditions depend for the hydrokinetic turbines. The output parameters of the hydrokinetic turbines have been analyzed based on the variation in the site conditions like flow velocity, free surface, blockage effect and bed forms.

The parametric analysis of Savonius (Cross Flow) hydrokinetic turbine is conducted using the Computational Fluid Dynamics (CFD), k-epsilon realizable model in its transient state. By fixing different parameters like blockage ratio, TSR, number of blades, Reynolds number and flow velocity, the effect of installation of the turbine at different installation (Clearance Ratio) conditions was analyzed. The turbine yields its maximum performance corresponding to 0.51 value of clearance ratio at 0.8 TSR. Further the effects of installation parameters have also been analyzed at different operating conditions (TSR).

ACKNOWLEDGEMENT

I would like to express my sincere gratitude to my guide **Dr. R. P. SAINI,** professor, HRED, Indian Institute of Technology Roorkee for his valuable guidance, support, encouragement and immense help. I would also express my deep and sincere gratitude to **Dr. S. K. Singhal**, Head, HRED, Indian Institute of Technology Roorkee for their motivation during the work of my dissertation.

I am very much thankful to research scholar Gaurav Saini for reviewing the work and support to improve the quality of the report. Moreover, I would remain grateful to all faculty members and staffs of Department of Hydro and Renewable Energy, Indian Institute of Technology, Roorkee and also would like extend my heartfelt thanks to all my friends who have helped me directly or indirectly for the completion of this dissertation. Finally, I would like to thank Ministry of Human Resource Development (MHRD), for sponsoring me for the course and of course my family members who had been continuous support for my studies.

RAJIV KUMAR TRIPATHI

CONTENTS

LIST OF FIGURES

LIST OF TABLES

CHAPTER 1

INTRODUCTION

1.1 GENERAL

In the next few decades, substantial increase in energy demand and electricity is expected due to propulsion of sustained economic growth and increase in income levels in India. There is a peak and an ultimate deficit of 0.8 % and 0.6 % respectively of energy in financial year of 2018-19. To maintain a GDP growth of about 6.6% per annum over the next few years, it is projected that India require about 7% growth of electricity supply after considering an elasticity of 0.82 in energy.

Energy demand has more than doubled since 1970. New technologies to 2060 will maintain moderate development in energy demand compared to historical trends, and will help allow industrialized economies to move faster into service and sustainability-led development. Efficiency gains will be achieved through the deployment of more effective power resources, coupled with the impact of digital technologies viz. intelligent grids, smart houses, intelligent homes and offices, and intelligent towns. Advanced production, automation, telecommunication and other techniques will also interfere with traditional energy systems [1]. The all India capacity of power stations in India is given in Table 1.1.

Table 1.1 Installed capacity of power stations of all India (in MW) (As On 31.08.2018) [2].

Region	Mode-wise breakup							Grand Total
	Thermal				Nuclear	Hydro	RES (MNRE)	
	Coal	Gas	Diesel	Total				
Northern Region	51985.20	5781.26	0.00	57766.46	1620.00	19707.77	13012.88	92107.11
Western Region	70608.62	10806.49	0.00	81415.11	1840.00	7547.50	20725.38	111527.99
Southern Region	45782.02	6473.66	761.58	53017.26	3320.00	11808.03	35535.49	103680.78
Eastern Region	27201.64	100.00	0.00	27301.64	0.00	4942.12	1075.85	33319.61
North Eastern Region	520.02	1706.05	36.00	2262.07	0.00	1452.00	286.46	4000.53
Islands	0.00	0.00	40.05	40.05	0.00	0.00	12.56	52.61
All India	196097.5	24867.46	837.63	221802.59	6780.00	45457.42	70648.61	344688.61

New clean energy generation is required to fulfill climate goals and utility company models are driven to the limit by rigorous policies and changing customer requirements. The sector needs to discover a way to navigate the changing dynamics. More strict regulatory demands for a future with low carbon emissions will force businesses to make important adjustments to their business models. This shift is especially pronounced for utilities that need to react rapidly to changing patterns of demand.

1.2 RENEWABLE ENERGY

Need of multiple energy services can be satisfied by several types of renewable energy sources which can produce thermal energy, supply electricity, and produce mechanical energy, and can also produce fuels. Some Renewable energy technologies are deployed within large energy networks which are centralized and some are deployed in rural and urban environments which are decentralized. Some renewable energy technologies are still at initial phase of technical maturity to support the markets commercially and some technologies are already matured technically.

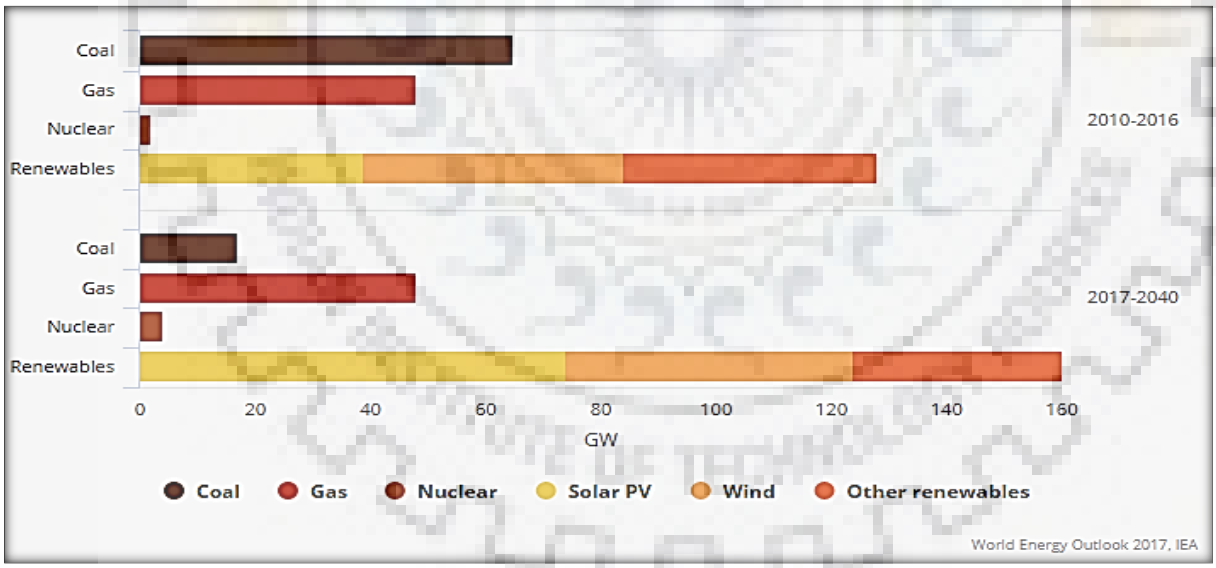

Fig. 1.1 Global average energy net additions by different energy sources [4].

India has renewable energy generation capability installed at 70648.61 MW as of 2018, and is anticipated to achieve 175,000.00 MW by 2022. India is the first nation in the world to set up a ministry for new and renewable energy across all nations in the world, and it represents the growth potential of renewable energy generation in India as shown in Fig 1.1. Looking at the view of renewable energy generation, India ranks fifth (after the United States, China,

Germany, and Spain). India requires to enhance the renewable energy contribution, as a serious issue in India turns out to be environmental degradation owing to air pollution. Fossil fuel-based energy been India's main factor for economic growth, and contributes in environmental air pollution is occurring in this phase. India ranks 3rd in the world (after China and the US) in carbon dioxide (CO_2) emissions. With the increase in economic growth, energy demand will increase in coming years, and these demand are both domestic and industrial. [3].

1.3 TYPES OF RENEWABLE ENERGY

1.3.1 Wind Energy

Compared to conventional fossil fuel based energy source, wind energy is a clean alternative source of energy and has the benefit of being exploited in rural and remote regions. Scientific wind mapping has been performed widely to tap the potential of wind power sources. India currently has an installed energy generation capability of just over 2078 GW, of which about 25 GW are renewable resources and most of this installed capability is wind. There is enormous activity in wind power, all over-India with an installed capacity of 22,465 MW. India currently has the world's fifth biggest installed wind capability. High-quality wind energy sites have a minimum capacity factor of about 25 percent at 80 m hub height and have a potential ranging from 253 GW (no farmland included) to 306 GW (all farmland included). In wind power generation, however, the plant load factor (PLF) is very small, often in single digits [4].

1.3.2 Solar Energy

Solar energy is an optimal source of energy as it is free and nearly unlimited. The solar radiation that reaching the surface of the earth in one year, supplies more than 10,000 times the annual energy requirements of the world. In addition, the use of only one-quarter of the solar energy that falls on the paved fields of the world could comfortably fulfill all present worldwide energy requirements. India is densely populated country which receives large amount of solar energy, an optimal combination for the use of this can solve India’s energy crisis. Because of its place between the Tropic of Cancer and the Equator, the average annual temperature of India is varying from 25 °C to 27.5 °C and is densely inhabited with elevated solar insolation. Therefore India has huge solar potential. India has targeted 100 GW of Solar power by 2022, driven by growing consumption of electricity and the gap between the supply and demand is widening day by day. With approximately 300 clear, sunny days in a year, India's theoretical solar reception is about 5000 PWh/year or about 600,000 GW only in its land region. The average daily event

of solar energy in India ranges from 4-7 kWh/m2 with around 1500-2000 hours of sunlight per year (place dependent), which is far more than the present complete energy consumption. [4].

1.3.3 Tidal Energy

India has a great ability to unravel this enormous sustainable and renewable energy resource. India has a lengthy shoreline of approximately 7500 km and about 336 islands in the Bay of Bengal and the Arab Sea with gulfs and estuaries where tides are powerful enough to drive turbines to generate electricity. The Gulf of Kutch and the Gulf of Cambay on the west shore of Gujarat have a maximum marsh area of 8 m^2 and 11 m^2 with an average marsh area of 5.23 m^2 and 6.77 m^2 respectively.

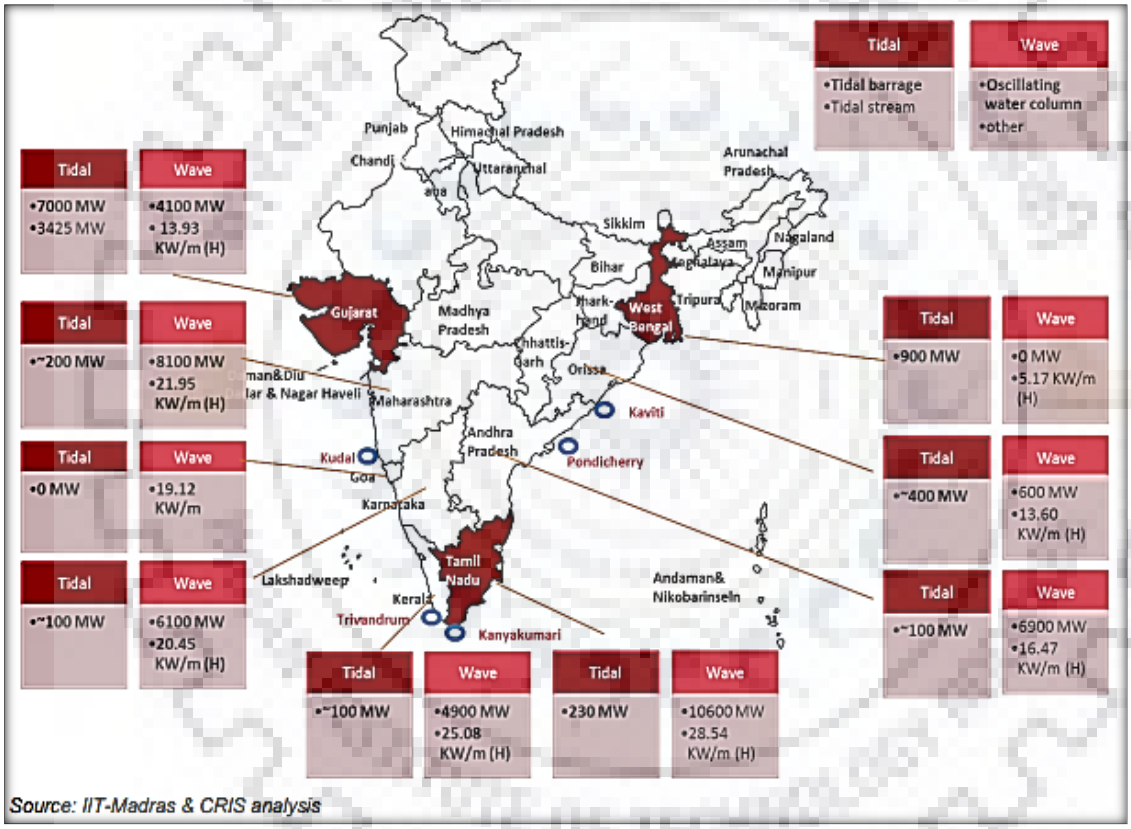

Fig. 1.2 State wise distribution of sites for harnessing wave and tidal energy in India [5].

The Sundarbans Ganges Delta is about 5 m with an average tidal range of 2.96 m. The recognized financial potential is approximately 8000 MW with almost 7000 MW in the Gulf of Cambay, 1200 MW in the Gulf of Kutch in Gujarat and approximately 100 MW in the Gangetic Delta in the West Bengal's Sunderban area [5].

1.3.4 Geothermal Energy

In 24 nations around the world, a number of geothermal power plants generating more than 10,000 MW are operational. In addition, in at least 78 nations, geothermal energy is used directly for heating. India has enormous potential to be a major contributor to geothermal energy generation. However in India, energy generation through geothermal resources is still in its nascent stages. In India, about 340 geothermal hot springs have been recognized.

Most of them lie in low surface temperature range from 37°C to 90°C, appropriate for direct heat applications. These springs are divided into seven geothermal Sahara Valley, Himalayan Cambay Basin, Son-Narmada-Tapi lineament belt, Godavari and Mahanadi basin and West coast. Some of the prominent geothermal reserves include Chhumathang, Puga Valley in Jammu and Kashmir, Manikaran in Himachal Pradesh, Jalgaon in Maharashtra and Tapovan in Uttarakhand. Tattapani in Chhattisgarh is a new geothermal energy site that has been most recently discovered [6].

1.3.5 Biomass and Biogas Energy

India is predominantly an agricultural economy, with enormous amounts of biomass fuel available in the form of straw, husk, cotton, jute, coconut shells, wild flowers, etc. Biomass is generated in nature by means of solar energy conversion through a process of photosynthesis. Biomass fuels used in India account for about one-third of the total fuel used in India, the largest fuel used in over 90 % of rural homes and around 15 % of urban homes. Despite advances in biomass energy technology, India still has the majority of biomass energy consumption restricted to traditional uses. Modern techniques allow the conversion of biomass into the synthetic gaseous or liquid fuel (such as ethanol and methanol) and then into electricity.

An estimated production of 350 million tons of agricultural waste annually, biomass can supplement coal with approximately 200 million tons of power generation. In bioenergy techniques such as gasifier, biogas, cogeneration, biomass combustion, cattle dung can be used to generate heat or electrical energy. The co-generation program for biomass energy is to be introduced with the primary goal of encouraging technological cogeneration for the optimal use of India's biomass cogeneration resources. The generation potential of the energy by the use of biomass in India is estimated to be about 30000 MW.

Table 1.2 Programme/Scheme wise Physical Progress of different renewable energies [5].

Sector	FY 2018-2019		Cumulative Achievements
	Target	Achievement (April-Dec 2018)	(As on 31.12.2018)
Grid interactive power (capacities in MW_P)			
Wind power	4000.00	1145.10	35288.10
Solar Power-Ground Mounted	10000.00	3994.38	24582.23
Solar Power- Roof Top	1000.00	380.11	1443.74
Small Hydro Power	250.00	42.25	4528.05
Biomass (Bagasse) cogeneration	250.00	374.70	9075.50
Biomass (non-bagasse) cogeneration/Captive Power	100.00	41.93	704.74
Waste to Power	2.00	0.00	138.30
Total	**15602.00**	**5978.47**	**75760.66**
Off Grid/Captive Power (capacities in MW_{EQ})			
Waste to Energy	18.00	6.58	178.73
Biomass Gasifiers	1.00	0.00	163.37
SPV Systems	200.00	171.70	843.11
Total	**219.00**	**178.28**	**1185.21**

1.3.6 Hydro Energy

Hydroelectric power plants transform water's potential energy into electrical energy. The hydroelectric power plant are constructed on a dam where the dam's height is used to generate potential water energy for electricity generation. The first hydroelectric power station of India was established at "ShivanaSamudra" in Karnataka.[6].

India's power consumption is the world's fifth highest. India's energy consumption has risen relatively rapidly in the last six centuries due to population growth and economic development, India's energy consumption has risen 70 times from 16 kWh (1947) to 1149 kWh (2018) per capita and from 136 GW in 1947 to 356 GW in 2018.

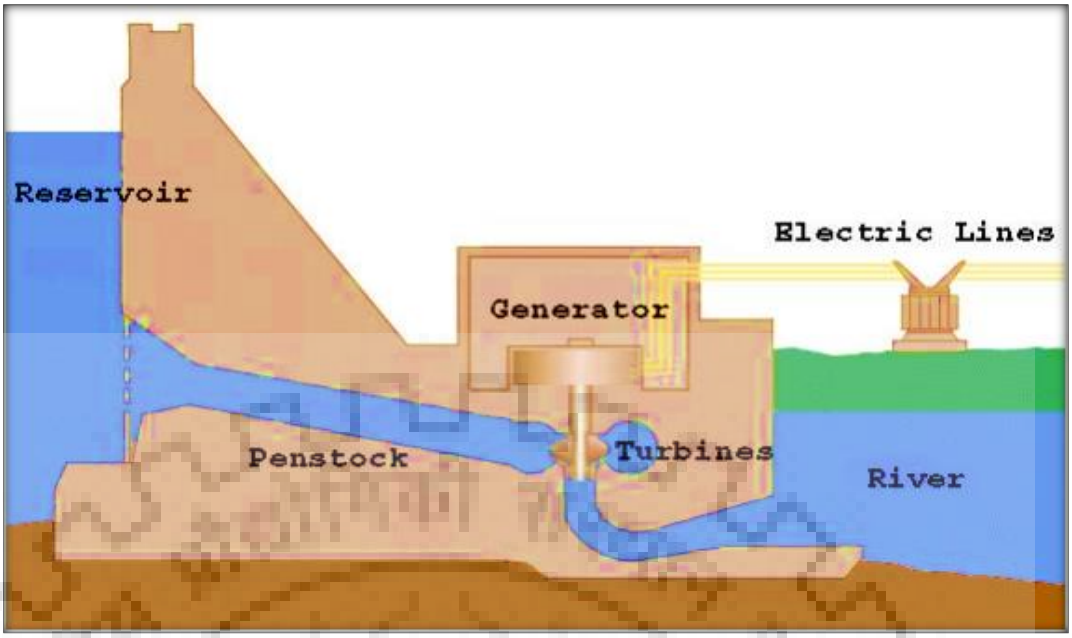

Fig. 1.3 Schematic of a Hydropower Facility [7].

1.4 HYDROKINETIC ENERGY

The energy possessed by the moving water is known as hydrokinetic energy. Hydrokinetic energy utilizes the kinetic head available in the water rather than the potential head which is converted in most of the conventional hydro turbines. Hydrokinetic power conversion technologies are electromechanical equipment that converts kinetic energy from tidal currents, river streams, man-made water channels or waves into electricity without using head and impoundment. Hydrokinetic conversion systems produce electricity by making the use of flowing water contained in tidal currents, river streams or other man made water ways. The main difference between conventional hydropower plants and the hydrokinetic energy technology is that the later one uses the speed of flowing water for the generation of electricity and the previous one uses head available on the site. For the generation of power by hydrokinetic turbine no head is required that is why this is also called "zero head" or "in stream turbine".

1.4.1 Working Principal of Hydrokinetic Turbine

Working principle of hydrokinetic turbine is similar to the wind turbines and both of them share the same principal in working and design. Only the parameter which differs is the density of water which is nearly 150 times the density of air [8].

Kinetic energy of flowing water is converted into electrical energy by a hydrokinetic turbine. The amount of energy contained in a river stream depends on cube of fluid velocity, area of cross section and density of fluid. The theoretical power extraction from a hydrokinetic turbine can be evaluated from the density of a fluid, the cross sectional area and the velocity.

$$C_P = \frac{P}{\frac{1}{2}pAv^3} \quad (1.1)$$

Where, P = Power in the flow

ρ = density of water (kg/m^3)

A = blade swept area (m^2)

V = velocity of water (m/s)

1.4.2 Classification of Hydrokinetic Turbines

Hydrokinetic turbines uses the kinetic energy of the flowing water and can be deployed in canals, rivers and irrigation systems. These turbines are totally different from conventional turbines.

Depending on the orientation of rotor axis with respect to the direction of incoming water these turbines are mainly classified in two categories.

i. Axial Flow Hydrokinetic turbines
ii. Cross Flow Hydrokinetic turbines

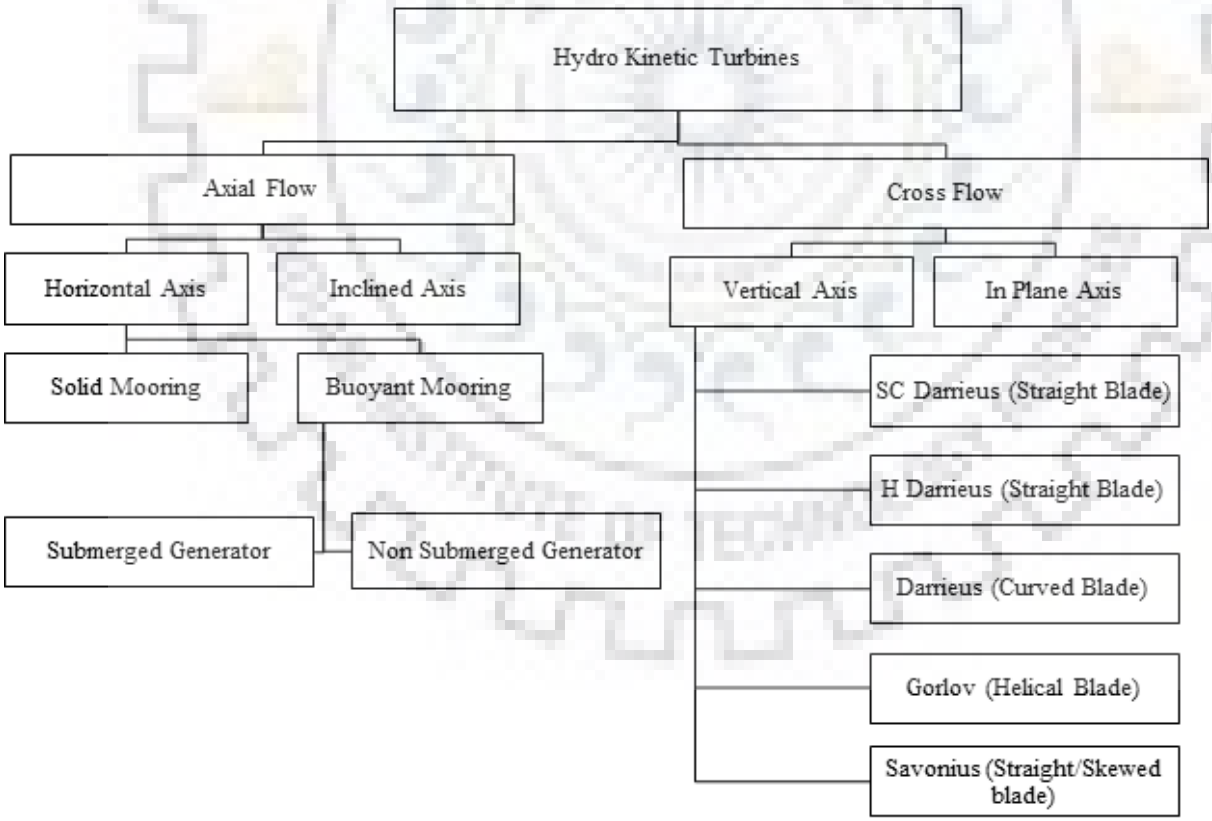

Fig. 1.4 Classification of the Hydrokinetic Turbines

1.4.3 Axial Flow Hydrokinetic Turbines

Those turbines which have their rotational axes parallel to the incoming water are known as axial flow hydrokinetic turbine. Axial flow hydrokinetic turbines have advantages like high efficiency, self-starting torque is low, and fluctuation of torque is minimum and can perform operations at high speed.

Inclined axis turbines were mostly researched for small river energy converters. Most of these instruments were tested in river streams and commercialized on a restricted scale. Axial flow turbines are popular in tidal energy converters and are very comparable from the concept and design point of view as compared to the conventional wind turbines. Different arrangements under the axial flow hydrokinetic turbine category are shown in Fig. 1.5.

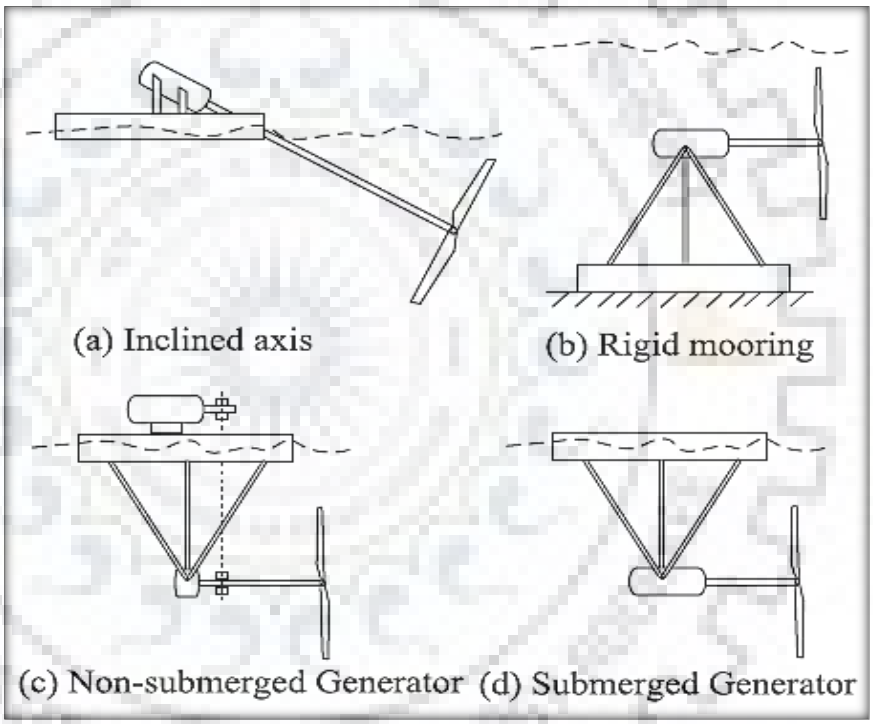

Fig. 1.5 Axial Flow Hydrokinetic Turbines [9]

Turbines with solid mooring structures require the generator unit to be placed near the riverbed or seafloor. Axial flow hydrokinetic turbines with a buoyant mooring system can allow a non-submerged generator to be positioned nearer to the water surface [8].

1.4.4 Cross Flow Hydrokinetic Turbines

Those turbines that have their rotor axis vertical to the water surface and perpendicular to the incoming water stream are called cross-flow turbines. The rotor axis of the cross flow turbines are perpendicular to the flow. The cross flow turbines are also referred as floating waterwheels [8]. These are primarily drag-based equipment and inherently less effective than their counterparts

based on the lift. Different arrangements under the category of vertical axis or cross flow turbines are shown in Fig. 1.6. The most prominent choices in the vertical axis turbine domain is Darrieus turbine. Although the use of Squirrel-cage Darrieus (straight bladed) or H-Darrieus turbine is very prevalent.

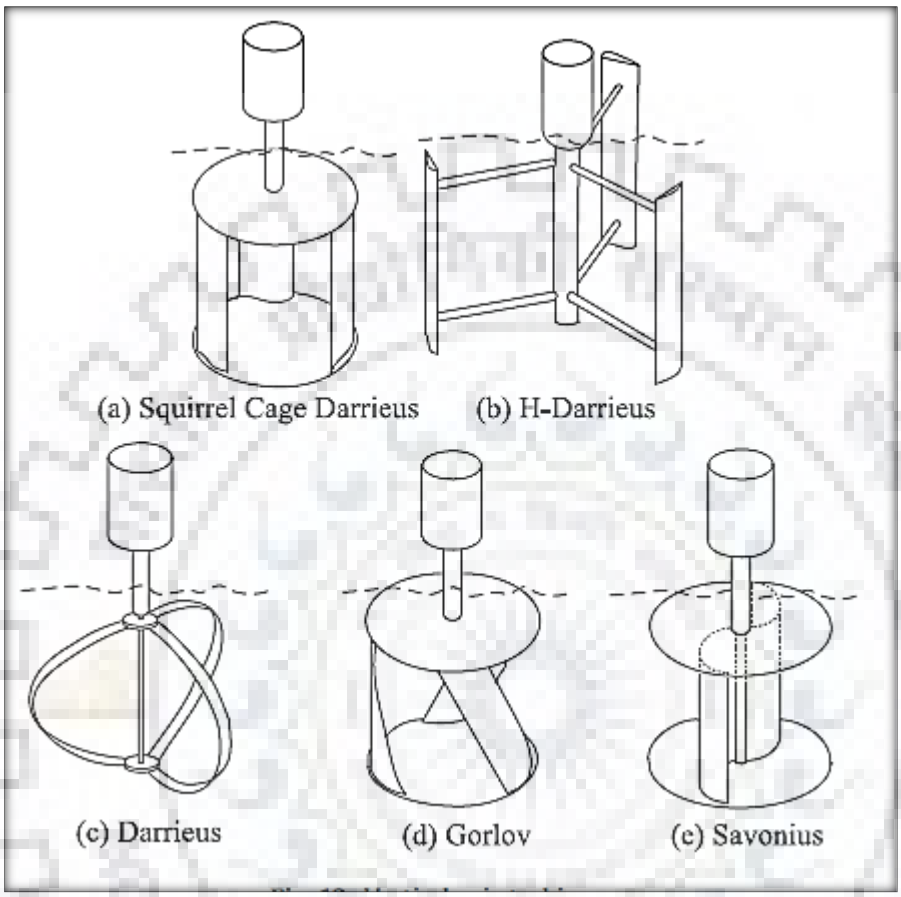

Fig 1.6 Cross Flow Hydrokinetic Turbines [8]

The Gorlov turbine is the other part of the vertical axis family, where it has helical structure of the blades. Savonius turbines are drag type devices, which have straight or skewed blades.

Comparison between the Cross Flow and Axial Flow Hydrokinetic Turbines based on different parameters is given in Table 1.3

Table 1.3 Comparison of Axial Flow and Cross Flow Hydrokinetic Turbines [8].

Parameters	Axial Flow Hydrokinetic Turbines	Cross Flow Hydrokinetic Turbines
Design	Design of the blade includes delicate manufacturing and machining.	Use of straight blades makes the design simple and cheap.
Generator Coupling	Can be achieved by a long inclined shaft, right-angled gear coupling, or underwater placement of the generator.	The generator can be placed in one end of the shaft, allowing the generator to be placed above the water surface.
Floatation and Augmentation Equipment	Use of ducts is difficult for floatation purposes.	Darrieus Turbine's cylindrical shape enables the easy mounting of multiple rectilinear or curvilinear ducts.
Noise Emission	Relatively emits more noise.	They emit less noise.
Skewed Flow	Less suitable	More Suitable.
Starting Torque	High	Low
Efficiency	High	Low

1.4.5 Advantages of Hydrokinetic Energy

There are a number of advantages that make hydrokinetic energy system distinct from other hydropower system. Some of the advantages are given below

a) Do not involve extensive civil works to be carried out.
b) Operates in the water stream natural pathway and does not require a diversion of flow stream.
c) Less noise and vibration issue than conventional turbine.
d) There is no requirement of hydraulic head difference.
e) There is no requirement of a dam or barrage for operation.
f) Reduction in environmental problems.
g) Hydrokinetic turbines used for harnessing the hydropower are fish friendly.
h) Low gestation period.

i) Negligible maintenance cost and low operation cost
j) Maximize the performance of hydropower plant by installation of hydrokinetic turbine at the downstream of the dam.

1.5 SITE DEVELOPMENT (PRE-FEASIBILITY AND FEASIBILITY STUDIES)

In the pre-feasibility stage of site growth, field surveys of the current physical setting should determine the overall features of the site. Field surveys should be carried out to determine the river's surface profile, water depths and current velocities for a range of discharges, and river bed bathymetry at chosen cross-sections within reach. In the pre-feasibility phase, a complete bathymetric survey of the entire reach of interest is not required, but in the feasibility study it will be needed.

A two-dimensional numerical model will provide data on the velocity and depth distribution of a range of discharges within reach to assist define the most appropriate areas for hydrokinetic turbines installation. The depth and velocity distributions at low flows are of specific significance for this new technology, as they are the limiting factors in determining turbine positioning and energy production.

During the feasibility study stage, final site features and precise turbine locations will be determined.

The site's primary benefits and disadvantages, including future technical and environmental problems will be determined in this project development pre-feasibility stage. A preliminary financial evaluation will also be carried out.

The most interesting locations determined from the pre-feasibility stage will be researched widely during the feasibility stage of site construction, which will require considerable investment and time. The objective of the feasibility study is to determine current and post-development hydraulic circumstances, carry out comprehensive engineering designs to allow an economic research, identify future environmental issues, receive the necessary governmental authorizations for site growth and create a maintenance and monitoring plan as well as performance indicators [10].

The feasibility stage involves, among other things:

a. Geological study of the river bed and banks.
b. Detailed bathymetric survey of the reach.
c. Measurements of the velocity profiles and water depths.
d. Detailed reconstituted hydrological series at the site.

e. A three-dimensional numerical model for a range of discharges of hydrodynamic conditions.
f. Optimization of the number of hydro turbines and their placement.
g. Study of interconnections with a current electrical grid.
h. Studies of the environment.
i. Model of economics
j. Civil structural design
k. Electrical and mechanical design of equipment.
l. Simulation of energy generation
m. Budget and timeframe.

CHAPTER 2

LITERATURE REVIEW

2.1 GENERAL

An extensive literature survey has been carried on hydrokinetic turbines particularly in the area to identify and understand the various performance parameters and site conditions in which these studies have been carried out and an attempt has been made to find out the scope for future work in the field of hydrokinetic turbines. In this chapter various literature and investigations have been studied to investigate the working of Hydrokinetic turbines under different flow conditions. Literature review in the hydrokinetic turbines is discussed in following fields.

1. Investigations of axial flow hydrokinetic turbines
2. Investigations of cross flow hydrokinetic turbines
3. Investigations of the literature on various/miscellaneous parameter of hydrokinetic turbines.

2.2 INVESTIGATIONS OF AXIAL FLOW HYDROKINETIC TURBINES

Anyi and Kirke [11] investigated the problem of clogging by the floating debris and modified the conventional hydrokinetic turbine by adding one more blade which swings forth and back along the plane of rotation. The final design was found to shed lengthy stingy algae and function usually where a performance coefficient of 0.25 was observed.

Noruzi et al. [12] analyzed and predicted the performance of a horizontal axis hydrokinetic turbine by considering the installation depth of the turbine. Variation of the velocity profile with the depth of installation is given in Table 2.1. The results showed that h/H<20% plays a significant role in the performance of the HAMCT (h=depth of the turbine from free surface H=Total depth).

Table 2.1 Inlet velocity profiles of HAMCT at different depths of installation

Depth of installation from surface(m)	Velocity Profile(m/s)
1.1	$1.7+\frac{A}{2}\sin\omega t$
2.29	$1.7+\frac{A}{2}\sin\omega t$
3.4	$1.7+\frac{A}{2}\sin\omega t$
4.50	$1.7+\frac{A}{2}\sin\omega t$
5.58	$1.7+\frac{A}{2}\sin\omega t$
6.72	$1.7+\frac{A}{2}\sin\omega t$

Riglin et al. [13] conducted an experimental study on three array configuration of multiple hydrokinetic turbines by using Reynolds Averages Navier Stokes equations. These three array configurations were

(i) Two units next to each other.
(ii) Two units on and off the river.
(iii) Two by two orientations that are not staggered.

Results of simulation conclude that operating the propeller units side by side is advantageous in order to ensure optimum energy output.

Chawdhary et al. [14] studied the wake characteristics of a TriFrame of axial-flow hydrokinetic turbines, the flow past a TriFrame of hydrokinetic turbines in an open-channel was studied using both numerical and experimental simulations. The turbulent statistics and mean velocity were estimated correctly following the TriFrame.

Zhen and Xiaoping [15] performed time dependent reliability analysis on the blades of a river based on axial flow hydrokinetic turbine. The findings indicate that the model will efficiently assess the reliability of a hydrokinetic turbine blade over a certain time period. Analysis revealed that the material strength and the river flow velocity makes the highest contribution to the likelihood of hydrokinetic turbine blade's failure.

Riglin et al. [16] studied characterization of a hydrokinetic turbine near the free surface. Depths from free surface to blade tip with respective Froude numbers of 0.71, 0.92, 1.04 and 1.31 were specifically designed to capture the transition from subcritical to supercritical flow conditions. A sharp decline in efficiency was noted at the critical Froude number (Fr=1.0). Results under subcritical circumstances showed reasonable agreement with earlier published single-phase findings where the turbine is presumed to operate in an infinite medium. The propeller-based turbine study was compared with experimental and numerical outcomes acquired for a traditional marine present turbine (MCT) under subcritical circumstances. As the flow became critical, the energy coefficient was expected to reduce by 32.2% and important wake-free surface interactions were observed.

Guney [17] presented the valid energy conversion system equations from water currents similar to the wind system. Existing measures have been provided with the aim of raising the performance coefficient.

Kinsey and Dumas [18] investigated the effects of channel blockage upon the performance of axial and cross-flow turbines with the aim of filling the gap in the literature on appropriate cross-flow turbine blocking corrections. This research proves that the efficiency of a turbine is considerably influenced by the amount of confinement encountered by the stream. It is found that the sensitivity to blockage depends considerably on the working conditions (tip speed ratio).

Hill et al. [19] conducted series of studies to investigate the interactions between comparatively large scale dunes and axial flow hydrokinetic turbines. The experiment was finished under clear water conditions to evaluate the impact of single and two turbine facilities on local scouring. Aligned and single turbine settings were noted to affect the topography of the bed only locally. The presence of both additional turbines and bed forms resulted in decreased performance of the turbine. The interactions between the turbine bedforms are enhanced by steeper or higher beds.

Vaz et al. [20] presented an strategy for optimizing cavitation-free hydrokinetic turbines under diffuser effect. The formulations are based on the classical BET, the primary addition being the minimum pressure coefficient as the criterion for avoiding cavitation on optimal hydrokinetic blades. The results show that diffuser techniques intensify the cavitation on the blades of hydrokinetic turbine.

Wang et al. [21] developed a axial flow hydrokinetic river turbine technology for local renewable energy applications. The rotor has a peak effectiveness of 25.2 percent at present river velocity of 0.8 m/s, pitch angle of 4 degrees and TSR of 6. It is ensured that the rotor output does not deteriorate in a relatively large range even if the present velocity changes or if the TSR deviates from the design values. Finally, the unsteady hydrodynamic behaviors of this turbine have been further evaluated.

Aghsaee and Markfort [22] investigated the effect of flow depth on the downstream wake conduct of a axial flow hydrokinetic turbine. It is observed that the mean velocity recovers more quickly for a deeper flow and the turbulence intensity recovers more slowly. In addition to the thrust coefficient and turbulence intensity, the ratio of the flow depth to the turbine diameter (H / D) is an important parameter related to the wake recovery rate.

Summary of the literature work for axial flow hydrokinetic turbines is given in Table 2.2.

Table 2.2 Summary of investigations of axial flow hydrokinetic turbines.

Author (s)	Objective	System parameters	Operating Parameters	Results
Anyi and Kirke[11]	To investigate the effect of clogging caused by the debris on the performance of small axial flow Hydrokinetic Turbines [Experimental].	Turbine radius = 0.4 m C_p = 0.25 TSR = 4	Width of the concrete channel = 2.1m Average depth = 1 m Average velocity = 1 m/s.	It has been found that by designing the swinging blades clogging by long stringy sticky water weed could be avoided which would easily clog the conventional Hydrokinetic turbines. The value of Coefficient of performance which it achieved was 0.25
Kolekar and Banerjee[23]	To study the effect of blockage due to boundary proximity effect from deformable free surface. [Experimental]	Number of blades = 3 Radius = 0.14m	A 0.61 m×0.61 m test section open surface recirculating water channel. Flow velocity = 0.5 m/s-0.9 m/s	Blockage ratio below 10% did not show any improvement in performance. There has been increase in blockage ratio improvement of the power coefficient up to 35%.
Pyakurel et al.[24]	To perform a Numerical simulation of a downstream turbine operating in the wake of upstream turbine. [Numerical].	-	Mean Flow velocity = 1.6 m/s	Power produced by the coaxially located turbine downstream was found to be increased due to higher turbulence levels.
Tewari and Kolmsi [25]	The paper presents an idea of using hydrokinetic power as a feasible solution in	Length: 3130 mm Width: 1600 mm Height: 2010 mm	Flow Velocity = 1.5 m/s-3.5 m/s Depth = 1.8 m	The paper presents possible installation sites for Hydrokinetic turbine technology. There is also an

	Uttarakhand to secure low impact and sustainable power for rural communities. [Analytical]	Rotational speed = 90-230 rpm Number of blades = 3 Rotor Diameter =1000 mm	Width = 50 m to 250 m	idea of integrating photovoltaic into a hybrid system that makes the scheme more flexible and efficient. The future research will define the precise potential of hydrokinetic energy in Uttarakhand with a thorough research of the features of the river in the Upper Ganga Basin and create a hybrid system model for this area.
Chawdhary et al.[14]	The study focused on the wake characteristic of triframe of a axial flow hydrokinetic turbines [Experimental and Numerical]	Rotor Diameter = 0.15 m Number of Blades = 3	Laboratory flume Width = 0.9 m Length = 8 m Average Depth = 0.28 m Flow Velocity = 0.27 m/s	The results of both numerical and experimental studies were compared. The turbulent statistics and the mean velocity were precisely projected in the wake of the Triframe.
Riglin et al [16]	The study presents characterization of the hydrokinetic turbine in a vicinity of the free surface. [Numerical]	Rotor Diameter = 0.5334 m Number of Blades = 2	Width = 0.5 m Depth = 0.3798 m Flow velocity = 0.334 m/s	The performance due to transition from subcritical to super critical flow was studied at Froude number of 0.71, 0.92, 1.04 and 1.31. There was a sharp decline in the performance at the critical Froude number (Fr=1.0). There was an acceptable agreement between the results at the subcritical level and the previously published single phase results where the turbine was assumed to be operating in an

				infinite medium. There was a decrease of 32.2 % in the power coefficient as the flow became critical.
Vaz et al. [20]	To present an approach for optimizing hydrokinetic turbines free of cavitation under diffuser effect. [Numerical]	Turbine diameter = 10.0 m Number of blades = 3 Submergence of the turbine = 6 m	Flow velocity = 2.5 m/s	The formulations are based on the classical BET, whose main addition being the minimum pressure coefficient as the criterion to avoid cavitation on optimum hydrokinetic blades.
Wang et al. [21]	A horizontal axis micro-hydrokinetic river turbine technology was developed for local renewable energy applications. [Experimental]	Number of blades = 3 Diameter = 2 m	Flow velocity = 1 m/s-1.5 m/s	The rotor has a maximum efficiency of 25.2% at a pitch angle of 4 degree, the river current speed of 0.8 m/s, and TSR of 6. The performance of the turbine does not deteriorate even if the current speed changes or the TSR deviates from the design values.

2.3 INVESTIGATIONS OF CROSS FLOW HYDROKINETIC TURBINES

Talukdar et al. [26] studied vertical axis helical bladed turbine by performing experiments for different immersion level of the turbine in water and concluded that the value of power coefficient drops drastically as the immersion level is increased i.e. C_p is maximum for fully immersed turbines.

Birjandi et al. [27] studied the fixed blockage ratio due to the adjacent turbines and variable free surface effect on the vertical hydrokinetic turbine. Results show that power coefficient increases as the water level decreases when the turbine is fully submerged. The power coefficient increases due to the free surface effect.

Fernandes and Rostami [28] experimentally investigated the feasibility of an innovative turbine model with a vertically hinged flat plate in the turbine axis. This turbine is called the vertical axis autorotation turbine that takes advantage of the autorotation phenomenon to harvest energy.

Kumar and Saini [29] performance of Savonius turbines having twisted blades using CFD analysis. An effort to optimize this turbine's twist angle was made. Result obtained from the analysis showed that Savonius hydrokinetic turbine with a twist angle of 12.5 provides a maximum power coefficient of 0.39 corresponding to a TSR value of 0.9 for water velocity of 2 m/s.

Sharma et al. [30] evaluated how the Savonius wind turbine performs when it rotates by the momentum of water current at low speed from 0.3 m/s to 0.9 m/s in an open water channel. The power and torque for the hydrokinetic turbines increases with the increase in free stream velocity, which is maximum for the velocity of 0.9 m/s. This, however, raises the load on the turbine blades, thus reducing the turbine's longevity. There is an optimum value of the TSR of 0.77 at which the maximum energy coefficient (Cp) of 0.39 is achieved, which is greater than the conventional Savonius wind turbine at the corresponding input values. At different levels of water the power extracted is inconsistent. The higher velocity gradient on the top layer results in the highest power extraction compared to the other layers. The turbine's higher power at the bottom layer than the middle layer is attributed to the shear layer separating from the channel bed. Therefore, its effect on power should not be considered in extracting design information about turbine performance.

Kirke [31] conducted a series of test on several Darrieus type hydrokinetic turbines. The experiments were carried out in Canada and Australia on HKTs with fixed and variable pitch

straight blade, fixed helical blade, with and without a slatted diffuser, by mounting the turbine in front of a barge and moving it through the still water at speeds of less than 1 m/s to 5 m/s. The diffuser improved the power by three times in one setup, but significantly less in others. The helical blades made insignificant difference to starting torque and efficiency but the turbine ran smoothly, unlike with fixed pitch straight blade. The diffuser increased the power output three folds for the same turbine without a diffuser.

Sharma and Sharma [32] estimated and compared the performance of a new configuration of Savonius turbine rotor with a conventional one, using numerical method. New configurations includes several quarter blades added to the conventional turbines. In comparison, new configuration was found to have better performance over the conventional configuration the different input velocity cases, reaching the maximum COP value of 0.226 for V = 8.23 m/s with an improvement of 8.89 %.

Forbush et al. [33] studied the performance characterization of the hydrokinetic turbine in the sheared inflow. A method for the construction of a non-dimensional performance curve for a hydrokinetic cross-flow turbine in the sheared flow is developed for the natural river site.

Talukdar et al. [34] investigated and evaluated the performance of the Savonius Hydrokinetic Turbine through numerical and experimental analysis. The SHT under investigation was developed in-house. Initially, the performance of the two and three-bladed SHT was compared with the conventional semicircular blades and the maximum power coefficients were found to be 0.17 and 0.28, respectively at tip-speed ratios of 0.67 and 0.84. Additional tests of a two-bladed SHT turbine with the elliptical blades showed its lower efficiency relative to the two-bladed semi-circular SHT. Comparison between the Darrieus turbine and Savonius Turbine based on different parameters is given in Table 2.3. Summary of the literature work for cross flow hydrokinetic turbines is given in Table 2.4.

Table 2.3 Comparison between Darrieus and Savonius Hydrokinetic Turbine

Parameters	**Darrieus Turbine**	**Savonius Turbine**
Tip Speed Ratio	High (more than unity)	Low(Less than unity)
Efficiency	High	Low
Self-starting characteristics	Poor	Good
Operation speed	High	Low
Working Principle	Lift force	Drag Force
Design	Simple	Complicated

Table 2.4 Summary of investigations of the cross flow hydrokinetic turbines.

Author (s)	Objective	System parameters	Operating Parameters	Results
Birjandi et al.[27]	To study the blockage effect due to adjacent turbines and the variable free surface effect. [Experimental]	$R_e=1.65\times10^5$ $R_e=2\times10^5$ $R_e=2.35\times10^5$ C_p vs TSR curves for different values of clearance coefficient	Water tunnel of dimension Width = 61 cm Depth = 60 cm Length = 183 cm Flow velocity = 1 m/s	Results show that power coefficient increase as the water level decreases when the turbine is fully submerged the power coefficient increases due to the free surface effect.
Kirke [31]	To investigate the effect of diffuser on the performance coefficient of a fixed and variable pitch straight helical Darrieus turbine [Numerical]	Number of blades = 4 Rotor Diameter = 1.2m	Diffuser present Width = 2.4 m Flow velocity =0.91 m/s	The diffuser increased power output by three times compared to the same turbine without a diffuser
		Number of blades = 3 Rotor diameter = 1 m	Flow velocity = 1.5 m/s-4 m/s	
Kumar and Saini [29]	The paper aims to study the performance of twisted blade Savonius turbine. [Numerical]	Number of blades = 2 Aspect Ratio = 1.58 Overlap Ratio = 0 Rotor Diameter = 0.160 m	Rectangular open Channel Height = 0.65 m Width = 0.55 m Length = 3 m Blockage Ratio = 0.12 Flow velocity = 0.5 m/s-2.0 m/s	The result of the simulation show that the coefficient of power of the turbine is found to have a maximum value of C_P 0.39 corresponding to TSR value of 0.9 at a twist angle of 12.5 at 2 m/s of water velocity

Talukdar et al.[34]	To investigate and evaluate the performance of the Savonius Hydrokinetic Turbine. [Experimental and Numerical]	No of blades = 2 (Semicircular) Aspect ratio = 1 Overlap ratio = 0.15 Diameter of blade = 144 mm	Water Flume Width = 0.1 m Height = 0.9 m Flow Velocity = 0.1 m/s – 6.1 m/s	A comparison of performance between two and three-bladed SHT with conventional semicircular blades has been carried out experimentally where their maximum power coefficients are found to be 0.17 and 0.28, respectively at their corresponding tip-speed ratios of 0.67 and 0.84. Further experiment with a two-bladed SHT turbine with elliptical blades have shown its inferior performance as compared to the two-bladed semicircular SHT
		No of blades = 3 (Semicircular) Aspect ratio = 1 Overlap ratio = 0.15 Diameter of blade = 144 mm		
		No of blades = 2 (Elliptical) Aspect ratio = 1 Overlap ratio = 0.15 Diameter of blade = 144 mm		
Sarma et al.[30]	The study aims to evaluate the performance of the conventional Savonius wind turbine at low velocities of water ranging from 0.3 m/s-0.9 m/s in an open water channel.	Number of Blades=3 Diameter of turbine = 0.26m Aspect ratio = 0.65	Open Channel Length = 12 m Width = 0.9 m Depth = 0.505 m Flow velocity = 0.03 m/s-2.5 m/s	The power and torque of the hydrokinetic turbine increases with increase in the free stream velocity which is maximum for the velocity of 0.9 m/s. The optimum value of TSR is 0.77 at which the maximum value of C_P = 0.39 is attained.

	[Experimental and Numerical]			
Fernandes and Rostami [28]	The study proposed a turbine that exploits the autorotation phenomenon and consists of a vertical axis of symmetry to harvest the power from the current. [Experimental]	Aspect Ratio = 1.66 Blockage Ratio = 0.21	Open Channel Length = 22 m Width = 1.4 m Depth = 0.75 m Flow velocity = 0.085 m/s-0.345 m/s	Two conditions shall be provided simultaneously in the VAACT in order to the rotation to be continuous.The first one is the adequate starting moment to overcome the inertia of rotation and the other one is the sufficient mass moment of inertia of system. Hence, to improve the rotational characteristic, this turbine implies extra moment of inertia by adding mass on the turbine blade.
Talukdar et al[26]	The study aims to evaluate the performance of NACA 0020 bladed helical turbines of different solidity ratio. The effect of solidity ratio is investigated on different turbines at different immersion levels.	Diameter of the turbine = 300 mm Height of the turbine = 300 mm Helix angle = 60 Chord length = 120 mm	Open channel flume Depth of the flume = 0.9 m Width of the flume = 1m Flow velocity = 0.8 m/s-0.87 m/s	The C_P has maximum value of 0.20 when it is fully immersed having velocity of 0.87 m/s at 1.02 TSR The value of C_P drops drastically as the percentage of immersion of turbine decreases.

	[Experimental]	Diameter of the turbine = 340 mm Height of the turbine = 300 mm Helix angle = 60 Chord length = 120 mm		
		Diameter of the turbine = 370 mm Height of the turbine = 300 mm Helix angle = 60 Chord length = 120 mm		

2.4 INVESTIGATIONS OF THE LITERATURE ON VARIOUS/MISCELLANEOUS PARAMETER OF HYDROKINETIC TURBINES

Lago et al. [35] discussed the advances in hydrokinetic systems explaining the hydrokinetic technologies which could be easily deployed in the rivers, ocean currents, tidal estuaries and also in constructed waterways (Canals). It explains how the Hydro Conversion Devices capture the energy of flowing water without impoundment or diversion of the conventional hydroelectric facility.

Petrie et al. [36] studied the techniques to quantifying the mean flow field using an Acoustic Doppler Current Profiler. The study focused on quantifying the hydrodynamics site, flow depth, average velocity, discharge etc.

Kolekar and Banerjee [23] studied the boundary proximity and blockage impact on turbines efficiency through computational and experimental studies. Results of computational experimental analysis for blockage effects, boundary proximity effects and Reynolds number dependency on performance and flow field of an MHkT is presented. Experiments were performed at different flow velocities on a laboratory MHkT within a 0.61 m or 0.61 m open surface recirculating water channel. CFD projections based on rotating reference frame techniques were consistent with experimental information. CFD study was further extended to understand the effect of blockage ratio and Reynolds number on the performance characteristics of the turbine. Increase in flow velocity resulted in an improved performance up to 0.7 m / s beyond which Cp versus TSR curve were found to be insensitive to the change in Reynolds number. Additionally, the effect of the blockage on turbines performance was examined by changing the sizes of the fluid domain for the laboratory model. The blockage ratio less than 10% did not have any significant impact on the turbines performance. Increasing the blockage ratio from 10% to 42% resulted in an increase in the operating TSR range with an increase of up to 35% in the power coefficients. Higher TSR values have greater blockage effects due to the faster rotational speed that leads to faster bypass flow and stronger wakes.

Anyi and Kirke [37] designed and constructed hydrokinetic turbine proposed for off-grid communities in Sarawak, Malaysia. It was established that the construction of an optimum hydrokinetic turbine blade can be completed by using simple jigs, common tools and common materials. This method reduces the cost of turbine significantly.

Ladokun et al. [38] assessed the feasibility and potential of increasing the hydropower production of Nigeria's three main hydropower stations by installing hydrokinetic turbines behind the

existing dams. The results showed that there is a considerable potential ranging in kilowatts and megawatts in each hydropower station.

Briand and Karen [10] studied on resource assessment and site development strategy for hydrokinetic turbine and concluded that hydrokinetic energy power generation is a viable solution particularly for Canada.

Neary et al. [39] studied and reviewed the mean velocity and turbulence intensity profiles for open channel flow. The experiment investigated different measured vertical profiles of longitudinal turbulence intensity and mean current velocity that have been reported for a large canal, medium-large rivers and laboratory flumes with classical models developed for turbulent flat plate boundary layer flows. The comparison suggests that a semi-theoretical exponential decay model and a power law can be used to provide first order approximation of the turbulence intensity and mean velocity profiles in rivers suitable for current energy conversion.

Birjandi et al. [40] studied and developed an innovative low cost hydrokinetic turbine site selection technique for low climate regions. This article introduced an innovative hydrokinetic site selection technique for cold climate regions using satellite imaging.

Tiwari [25] presented the concept of using hydrokinetic energy as a feasible alternative to ensure low impact and sustainable power for rural populations in Uttarakhand. The upper Ganga section from Gangotri to Rishikesh could be the best possible location to harness hydrokinetic energy. They presented an idea of integration of photovoltaic to form a hybrid system to make the system more flexible and reliable. Hybrid system combines hydrokinetic energy and photovoltaic for separate load profiles. With a thorough study of the features of the upper Ganga basin, future research will define the precise potential of hydrokinetic power in the UK and create a hybrid system model for this region.

Kusakana and Vermaak [41] investigated the possibility of using and developing hydrokinetic energy to supply affordable, sustainable and reliable electricity to isolated, remote and rural areas in South Africa where reasonable water resource is present. Hydrokinetic power simulations were conducted with HOMER software with a rural household and a BTS load as case studies under distinct energy and demand resources. The findings have been compared with those from a standalone PV system, diesel generator and wind turbine while all supply the same load. The criteria for comparison were the Total Net Present Cost, the Initial Cost, and the Cost of Energy.

In short, hydrokinetic energy generation is the best production alternative compared to the wind, diesel generator and PV where sufficient water resources are accessible.

Kinsey et al. [42] presented and tested a new concept for hydrokinetic turbine with oscillating hydrofoils to extract energy from water current. Results of this campaign showed that the prototype, and thus the oscillating hydrofoil concept, presents a good energy extraction potential with performance similar to rotating blades technology. Indeed, the effectiveness of hydrodynamic energy extraction reaches up to 40% for the current dual-hydrofoil turbine in tandem setup.

Motley and Barber [43] numerically examined the capabilities of passive pitch control of marine hydrokinetic (MHK) turbine blades under both instantaneous and long-term variable amplitude loading with consideration for practical design and operational constraints. Passively controlled blades that increase energy capture were shown to result in higher blade loads and increased required active control range, while those blades that decrease energy capture were shown to result in lower blade loads and decreased active control requirements.

Gorbena et al. [44] presented a different approach for the turbine array layout optimization problem. Two variations of Polynomial and RBF surrogate methods are employed to fit an objective function dependent on two variables longitudinal and lateral spacing. The methodology is applied to two different scenarios, considering uniform and non-uniform flow, with the objective to assess the capacities of each surrogate. As a consequence of having a greater number of turbine rows, results from the surrogate fitting validation evidence a greater sensitivity of the response results for staggered layouts than for inline ones.

Garcia et al. [45] presents a combination of both forms of electricity generation, photovoltaic generators and river turbine, to configure a hybrid system together with a subsystem of support based on hydrogen and batteries to guarantee the electrical supply of a set of isolated loads. The complete design of a hybrid system satisfies the energy requirements of a load. The methodology includes the optimal location of the turbine in a cross section of the river to maximize the performance of the hydroelectric generator, and the techno economic study of all components of the hybrid system for an efficient use of renewable energy resources. The results show that the hybrid system provides the power demanded by the loads, hydroelectric and solar photovoltaic generation are optimized, and the battery storage subsystem loading status is kept avoiding deep discharges. Summary of the literature work on various/miscellaneous parameter of hydrokinetic turbines is given in Table 2.5.

Table 2.5 Summary of investigations on various/miscellaneous parameter of hydrokinetic turbines.

Author (s)	Objective	System parameters	Operating Parameters	Results
Birjandi et al.[40]	To study a novel and low-cost satellite imaging technique for the selection of hydrokinetic sites in cold climates like central and northern Canada	-	Winnipeg River (Canada) 34 locations were assessed Average velocity = 2.05 m/s Average depth = 12.3m	Results showed that this technique is a powerful initiation to find prospective locations for the positioning of hydro-kinetic turbines and would significantly assist isolated communities replace their fossil fuels.
Petrie et al.[36]	The study focuses on quantifying the site hydrodynamics	-	Roanoke River (USA) Discharge = 556 m^3/s Area = 716 m^2 Average Velocity = 0.78 m/s Average Depth = 7.1 m	The discharge and the bulk velocities were predicted and measured and it showed a difference of about 5 %
Briand and Ng [10]	The paper focuses to develop and design a hydrokinetic site in the riverine environment,.	-	River Min. Velocity = 1.5 m/s Min. depth = 4m	The paper presented the various stages to assess the site conditions and its relevance for installing hydrokinetic turbines
Kusakana and Vermaak [41]	The paper investigates the possibility of using and developing hydrokinetic energy to supply sustainable, affordable and reliable electricity to	-	River Min. Velocity = 1.41 m/s Depth = 1.8 m Width = 5.2 m	Simulations of the hydrokinetic power have been performed with HOMER software with a rural household and a BTS load as case studies under different energy resources and demand. The findings

	isolated, remote and rural locations in South Africa where reasonable water resources are available.			are compared with those from a standalone PV system, wind turbine and diesel generator while all supply to the same load. The criteria for comparison were the Total Net Present Cost, the Initial Cost, and the Cost of Energy. In short, hydrokinetic power production is the best production alternative compared to the wind, diesel generator and PV where sufficient water resources are accessible.

2.5 GAPS IDENTIFIED

An extensive literature review have been carried on hydrokinetic turbines particularly in the area of cross flow hydrokinetic turbines to identify and understand the various design parameters in which study has been carried out and an attempt has been made to find out the scope for future work in the field of hydrokinetic turbines. Based on literature review the following gaps have been identified.

1. There have been few works on the immersion level of the hydrokinetic turbines relating to their performance coefficient (C_p).
2. Future work should aim at the integration of the turbine solidity in the blockage correction. This requires performing simulations over a broader range of turbine solidities. The applicability of these blockage corrections when a support structure is present should be investigated as well.
3. Effect of the free surface on the working of hydrokinetic turbines when operating in shallow water.
4. Few work have been reported in with reference to the performance of the hydrokinetic turbines under different site conditions.
5. There is a problem of debris attaching to the turbines and very less work is done in this area particularly relating to the hydrokinetic turbine. These limit their applications in tropical countries where a large amount of debris constantly drifts in the rivers.

2.6 OBJECTIVES

Based on Literature and identified gaps, it is found out that a lot of numerical and experimental investigations were carried out to improve the performance of hydrokinetic turbines. However very few studies have been reported to investigate the performance of hydrokinetic turbines under different site conditions. Therefore the objectives of the present study is to

1. To study different performance parameters of the hydrokinetic turbine.
2. To survey and analyze the site conditions of the work done on hydrokinetic turbines through literature survey.
3. To study the effect of different site parameters on the performance of hydrokinetic turbines.
4. To investigate the effect of depth of installation and Tip speed Ratio (TSR) on the performance of the turbine through Numerical analysis of Savonius Hydrokinetic Turbine.

CHAPTER 3

PERFORMANCE INVESTIGATION OF HYDROKINETIC TURBINES

3.1 GENERAL

The study of system parameters of the hydrokinetic turbines needs to be investigated. The site conditions involving both river (in stream) and tidal applications have also been studied and discussed thoroughly. Based on the site parameters the present work aims to find the performing characteristics of Hydrokinetic turbines

3.2 SYSTEM AND WORKING PARAMETERS

a) **Solidity (σ):** It is defined as ratio of effective area occupied by the blade to the total frontal area of the rotor.

$$\sigma = \frac{nC}{\pi D} \tag{3.1}$$

Where, n = number of blades, C = Chord length of the blades, D= Diameter of Darrieus turbine rotor.

b) **Power coefficient (Cp)** = Power coefficient (Cp) is the ratio of mechanical power developed by the turbine rotor to the actual hydrokinetic power available in the projected area covered by rotor.

$$Cp = \frac{Po}{\frac{1}{2}\rho A V^3} \tag{3.2}$$

Where, Po = Mechanical power available at turbine shaft, ρ = density of the working fluid,

$$A = H \times D \tag{3.3}$$

Rotor Area, H = Height of the turbine blade. Mechanical power developed by the rotor (Po)

$$Po = T \times \omega \tag{3.4}$$

T = Mean torque available at the turbine shaft, ω = Angular velocity of blade.

c) **Tip speed ratio (TSR):** It is defined as the ratio of peripheral velocity of the rotor to the free stream velocity of water.

$$TSR = \frac{R\omega}{V} \tag{3.5}$$

Where, R = Radius of turbine rotor

d) **Blockage ratio (BR):** It is defined as the ratio of the area covered by the rotor of the turbine to the projected flow area in the water channel.

$$BR = \frac{H\ D}{Hw\ Ww} \quad (3.6)$$

Where, Hw = Water depth height in channel, Ww = width of the water channel.

e) **Aspect ratio (AR**): It is defined as the ratio of height of the turbine rotor to the diameter of the rotor.

$$\mathbf{AR} = \frac{H}{D} \quad (3.7)$$

3.3 HYDROKINETIC TURBINE DESIGN PARAMETERS

3.3.1 Operations Principle

The operating principle of hydrokinetic turbine is similar to that of wind turbine. The power output of turbine is affected by mainly three factors, viz. swept area, free stream velocity and overall efficiency of conversion system. Maximum power available (P) in free stream can be calculated as follows

$P_o = 1/2\rho AU^3$ (3.8)

Where the power produced (P) by the Hydrokinetic turbine is as follows

$P = 1/ 2\rho AU^3 4\alpha (1-\alpha^2)$ (3.9)

$\alpha = (U-V_1)/U$ (3.10)

Finally, power coefficient (C_p) or performance coefficient is given as follows

$C_p = P/P_o = 4\alpha (1-\alpha^2)$ (3.11)

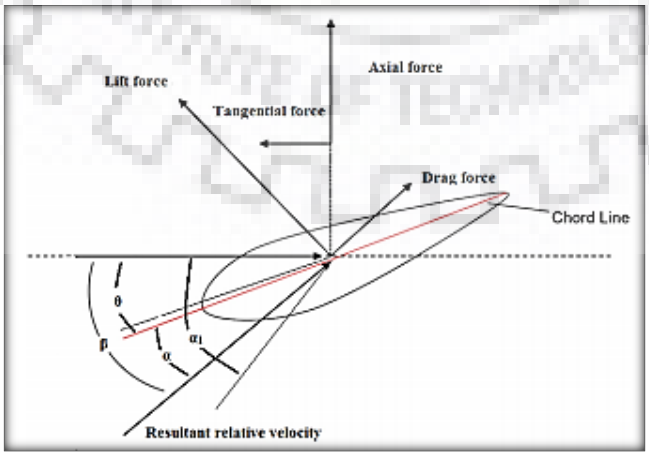

Fig 3.1 Force vector diagram and Velocity vector diagram on the blade element

In the above equations U, A, ρ, V_1 are free stream velocity, water density, turbine swept area, and water velocity at plane of rotor.

By differentiating the above equations with respect to α, and equating it to zero, maximum C_p or C_{pmax} is obtained as 0.59 i.e. maximum efficiency of turbine. This maximum C_P is also known as Betz limit.

The other important parameter that influence the performance of Hydrokinetic turbine is Torque coefficient (C_t) and is defined as the ratio of shaft torque at highest efficiency.

$C_t = 4T / (\rho U^2 D^2 H)$ (3.12)

Further, following relationship between C_t and C_p has been found

$C_p = TSR \times C_t$ (3.13)

$TSR = \omega D / (2U)$ (3.14)

Where TSR is tip speed ratio. Different forces on the hydrokinetic turbine blade also influences the performance viz. lift force (D_l) that acts perpendicular to the direction of flow, thrust force (D_{th}) or axial force that acts along axial direction and Drag Force (D_f) that acts parallel to direction of flow. Consequently, Lift coefficient (C_l), thrust coefficient (C_{th}) and Drag coefficient (C_d), can be formulated as follows.

$$C_d = \frac{D_f}{0.5\rho A(U-u_1)^2} \quad (3.15)$$

$$C_l = \frac{D_l}{0.5\rho A(U-u_1)^2} \quad (3.16)$$

$$C_{th} = \frac{D_{th}}{0.5\rho A(U-u_1)^2} \quad (3.17)$$

Where u_1, A, D, H, ω, U and ρ are rotational speed, turbine swept area, diameter, height, angular velocity of rotor, free current velocity and water density respectively.

3.3.2 Sizing of the Turbine Blade

Turbine blade sizing starts with the estimation of the available power potential given in Eq.3.18. The blades length or radius of Hydrokinetic turbine can be calculated from the following sets of Eqs. 3.19

$$P = \frac{1}{2}\rho A U^3 C_p C_n \quad (3.18)$$

In the above equations, C_n is derive train efficiency, C_p is coefficient of power, U is free stream velocity, ρ is water density, A is turbine swept area and P is power developed by hydrokinetic turbine. The pitch angle (θ) and chord length (t) of the turbines blade can be calculated from

the following Eqs. 3.19 and 3.20. The, angle of attack, relative velocity inlet angle and coefficient of lift calculated from Eq. 3.21 respectively.

$$t = \frac{16\pi r \sin\left(\frac{\alpha_1}{3}\right)^2}{C_1} \quad (3.19)$$

$$\theta = \beta - \alpha \quad (3.20)$$

$$\beta = 2\alpha_1/3 \quad (3.21)$$

Where r, α_1 and β are the radius, inlet angle and relative velocity inlet angle of local blade elements respectively. The above mentioned angles in the schematic diagram as shown in Fig. 3.1.

The angle of attack (α) depends on the azimuth angle and preset angle of attack can be calculated from the Eq.3.22.

$$\alpha = \theta_1 - \arctan\left\{\frac{\sin\theta_1}{\frac{1}{TSR}+\cos\theta_1} - \omega_1\right\} \quad (3.22)$$

Where ω_1 and θ_1 are preset angle of attack and azimuth angle.

Geometry design of the turbine blade can be done after obtaining the radius or length of the blade, pitch angle distribution, chord length distribution and the shape of the blade.

3.4 SITE CONDITION FACTORS FOR HYDROKINETIC TURBINES

3.4.1 Directionality of the Flow

The flow in the rivers is unidirectional and therefore there is no need for the rotor yawing. In tidal stream, a turbine has to operate both during low and high tides, therefore pitch/yaw mechanism is required for smooth operation.

3.4.2 Placement of the Hydrokinetic Turbines

The placement of the turbine in the water channel/body plays a significant role in obtaining optimum performance. Cross section of the channel decides whether a river or tidal current turbine can only be placed on the riverbed/seafloor in other arrangements (mounted or floating to a near-surface structure). Water velocity has a site-specific and highly localized three-dimensional profile and rotor positioning for such variations will determine the amount of energy that can be extracted effectively. Three classification of mounting arrangements are:

(i) Bottom Mounted Structure

(ii) Floating Structure Mounted (Buoyant)

(iii) Near-surface Mounted Structure (Fixed).

Different mountings for the turbines are:

Pontoon

1. Used in inland rivers as the water level varies significantly.
2. It allows the unit to be moved to an appropriate location where the water velocity is higher and there is not too many floating debris.
3. The turbines can be easily moved back to the river bank for maintenance or parking to avoid strong currents during flash floods.
4. They are cheaply and easily made.

Pivot arms

1. Generally used in rivers having small width by means of a level pivot arm.
2. Ease of maintenance and operation without the need of send the man into the water.

Bridge or Jetty

1. The turbine is suspended from a jetty or bridge using a long pole.
2. Installation is easier and less expensive as it is suspended from the bridge.

3.4.3 Water Density

The density of water varies from place to place. The water density at sea is higher than fresh water body. This means reduced ability of power generation for a tidal turbine when placed in river stream. Depending on the temperature and level of salinity, seawater in different time and location may have varying energy content.

3.4.4 Resource Prediction

Tidal conditions can be forecasted and easily accessible charts can be used for the coordination of the operation of a tidal power plant. The forecast of flow conditions is more engaged for river application and many geographical places may not have such agreements such agreements. Flow velocity decides the level of output for a hydrokinetic converter. Volumetric flow analysis is available at many places, but velocity of water differs from one potential to the other based on the cross-sectional areas. Therefore a correlation exists between the site bathymetry and flow variations needs to be reached for the turbines to be operated optimal performance.

3.4.5 Channel Morphology

The morphology of tidal channels and natural rivers is a complex one compared to the engineered channel, which can include power, drainage and irrigation canal. Measurement of hydrodynamics and bathymetry is therefore challenging. Natural channels typically have mobile boundaries composed of substrates ranging in sizes from fine clay, with a grain size of half a micron, to very large boulders with median grain sizes that equal or exceeds 4 meters in size. Four basic types of natural channel based classified on the median grain sizes of the bed substrates and channel slope or water discharge are

1. Sinuous uniform
2. Sinuous point bar
3. Point-bar braided
4. Bar- or island braided

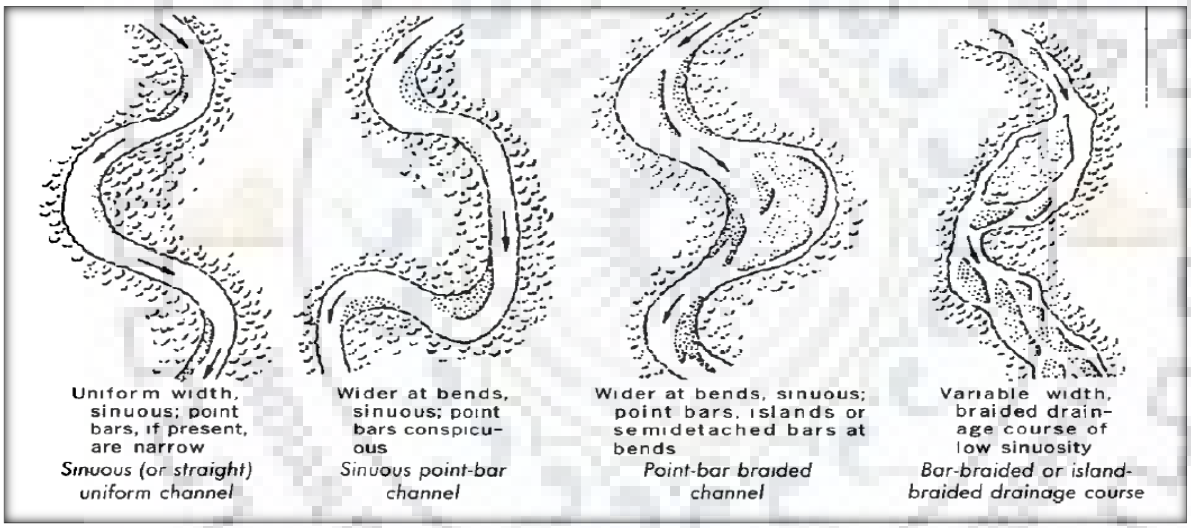

Fig. 3.2 River Channel Type [46]

Different types of river channels are shown in Fig. 3.2. Rivers and tidal channels that are regulated and unregulated are rarely uniform along their reaches. Natural channels are non-uniform in plan, section and profile and are rarely straight over twenty channel widths. These type of channels result in super-elevation of the water surface around the bends which can generate mixed water profile, deceleration of the bulk velocity, convective acceleration and strong secondary circulation. Channel geometry, mean-section depth, bulk velocity and mean-section depth typically changes along the length. In addition to difficulties in characterizing the variation of the local mean flow and bulk flow properties of tidal and river channels can be highly three-dimensional as a result of the variations in vortex shedding from river alignment and in stream structures.

3.4.6 Flow Variability in Rivers

There is a significant difference in the flow characteristics of river stream to that of tidal water bodies. While the sea has fluctuations relating to periodic nature (semidiurnal to diurnal), the river has strong annual variation (daily to seasonal). In addition, the stage of a stream may have different profiles for the two cases. Classical model assume constant uniform flow, but unregulated rivers have large variations of depth and discharge over time ranging from minutes to days based on the drainage basin size. Discharge of the regulated rivers like tail waters below hydropower dam, may change in minutes, but exhibit flow variability and less discharge than regulated rivers.

River may have extreme variation in measurements, flow and stage in the order of several decades which are typically needed to obtain meaningful statistics on the flow variability. Due to prohibitive expenses and instrument constraints, it is not practical for instrument deployments to extend the return periods observed in rivers.

3.4.7 Tidal Currents and Tidal Variability

The gravitational pull of the moon and sun on the earth's oceans leads to the tidal variations which causes tidal currents. These currents are relatively weak in the open ocean but in coastal environments the relative constrictions increases the peak current. The currents are generally aligned to the principal axis on flood (water flowing outwards) and ebb (water flowing inwards) at the sites of the hydrokinetic interest.

3.4.8 Turbulence and Velocity, Magnitudes and Distributions

During period of quasi-steady and steady flow, it is showed that Reynolds stresses and vertical velocity profile generally follow classical laws if large obstructions and roughness effect that disturb the boundary shear flows are absent. The mean velocity increases as it reaches near the free surface from the channel bottom.

3.4.9 Effects of Variation of Depth in Rivers

Fig. 3.3 illustrates the impacts of depth variation on the location of the energy extraction area and its centerline relative to the characteristic turbulence and velocity profiles. The hydrokinetic turbine at sites with high range of depth variations is compared to a tidal location where the variation in depth is much less pronounced. In theory, turbulence distributions and the normalized velocity would remain unchanged with flow changes and depth.

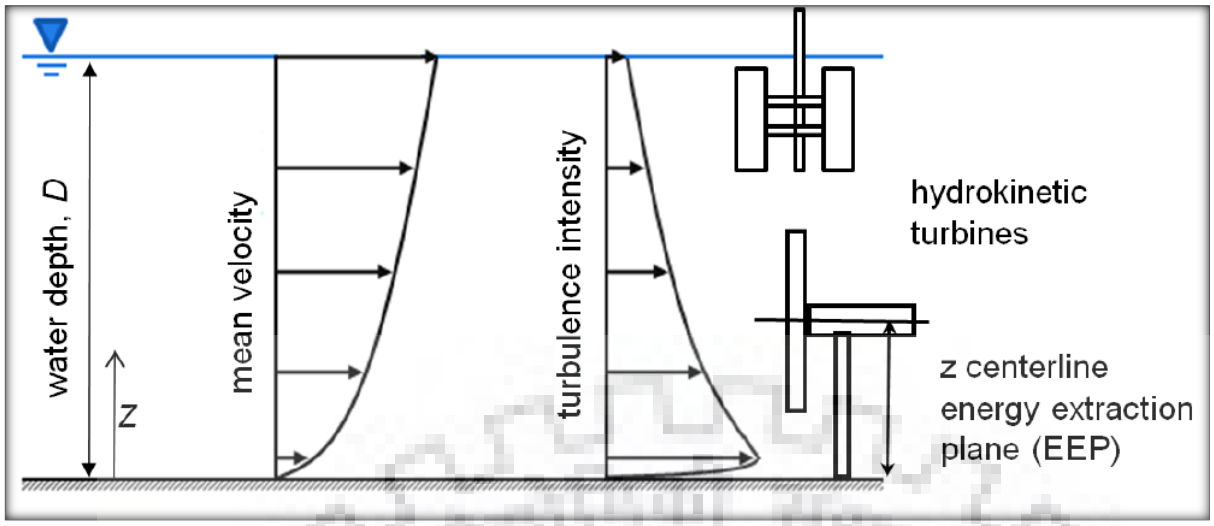

Fig. 3.3 Typical Distribution of turbulence and velocity profiles [39]

3.5 HYDROKINETIC TURBINES SITE PARAMETERS

3.5.1 Free-surface Effect

Few operational river and tidal turbine are tested in the field. Practically all the hydrokinetic turbines operating in the actual sites are subjected to effect of free surface. A non-dimensional (C_h) parameter clearance coefficient is proposed to understand the effect of free surface.

$$C_h = \frac{H}{L} \tag{3.23}$$

Where

H = height of water level above the turbine

L = blade height for vertical turbine and rotor diameter for horizontal turbines.

The positive clearance coefficient means that the water level is above the turbine blades; negative clearance coefficient means that the water level is below the top of the blade

3.5.2 Turbulence

The Reynolds number of a flow is used to classify a flow regime as turbulent or laminar; generally turbulent flow fields are characterized by their irregular flow field conditions. Temporal and random spatial variations, and non-linear governing equations. Given the environmental conditions of rivers, turbulent flow regimes are predominately present. Turbulent flow can be divided into an average component and a fluctuating component according to Reynold's Decomposition,

$$U=\bar{v}+u \quad (3.24)$$

Where U is the instantaneous flow velocity $\bar{v}$ is the average velocity, and u is the fluctuating component.

The energy distribution of the fluctuating component is governed by the energy injected by the mean flow, cascading down the length scales from the large Taylor-Marco scales down to the small Kolmogorov scales, and finally the viscous dissipation, which converts the kinetic energy into thermal energy. The large length scales are determined by the physical scale of the flow domain while the small scales are set by the viscosity of the fluid and the dissipation rate. The turbulent kinetic energy (TKE) is a summation of the fluctuating components of the flow according to:

$$T.K.E = \frac{1}{2}[u_x+u_{y+}u_z] \quad (3.25)$$

The amount of TKE in the flow can be determined by the use of transducers whose operating frequency exceeds the temporal frequency of the eddies present. Once the TKE is obtained it can be mapped along the channel, this provides a visual representation of the TKE flux along a flow path, around obstacles and other regions of interest. This technique is utilized here in order to qualitatively observe the effect of disturbances in the flow and recovery of the flow average velocity downstream.

3.5.3 Blockage Ratio

With the given geometry of the turbine and channel, the blockage ratio is a function of the projected area seen upstream/downstream of the flow and the RPM of the blades. The physical geometric blockage ratio fluctuates between the limits of where the turbine acts as a cylinder and does not let any water through, and the turbine being at a standstill where the minimum projected area is determined by the blade thickness. This is given in equation 3.28

$$\text{Blockage Ratio} = \frac{A_{turbine}}{A_{channel}} \quad (3.28)$$

where $A_{turbine}$ is the projected area of the turbine and $A_{channel}$ is the test domain cross-sectional area. Due to the large variability of the blockage ratio and dependence on the power output, it was not taken into consideration and instead assumed that the turbine would be operating in similar conditions in site locations where multiple HT turbines would be deployed in parallel to each other and experience wall effects from neighboring turbines.

The theory to predicting the power of turbines with high blockage ratio was given by Garrett and Cummins. This happens if a single turbine is deployed in a narrow channel or turbine array blocks the waterway. The theory also neglected the drop in the free-surface behind the turbine. The theory given by Garrett and Cummins was expanded by Whelan et al. for the Betz one-

dimensional analysis for shallow water applications. Fig. 3.4 shows the effect of the free surface on a turbine working in a shallow water.

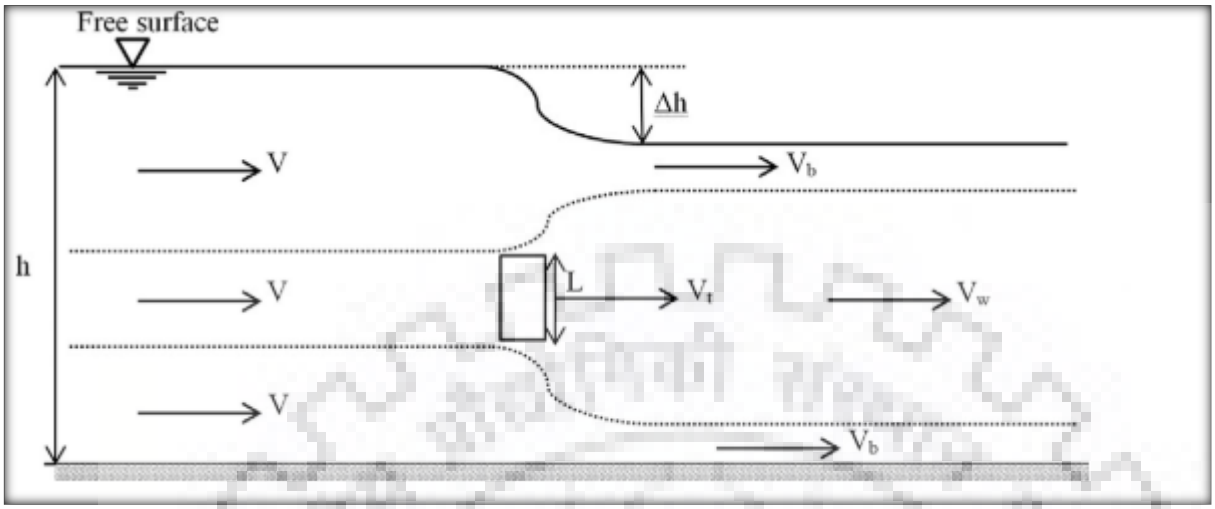

Fig 3.4 Schematic view of the one dimensional control volume [27]

Applying Bernoulli equation and continuity Whelan et al. developed a quadratic polynomial solution for a turbine with the height L situated in water depth h

$$F_r^2\tau^4 + 4\varepsilon F_r^2\tau^3 + (4B - 4 - 2F_r^2)\tau^2 + (8 - 8\varepsilon - 4F_r^2\varepsilon)\tau + (8\varepsilon - 4 + F_r^2 - 4\varepsilon^2 B) = 0 \quad (3.27)$$

Where

$F_r = \frac{V}{\sqrt{gh}}$ is the upstream Froude number

ε = ratio of the far wake velocity to the free velocity V_w

τ = ratio of bypass flow velocity V to free stream velocity

B = blockage ratio

3.5.4 Reynolds Number

Reynolds number is a dimensionless quantity which represents the physical properties of the flow. The increase in Reynolds number signifies increase in turbulence of the flow. The ratio of inertial force to viscous force is known as Reynolds number and this non-dimensional parameter is used to predict the flow conditions i.e. laminar or turbulent. If the inertial forces dominate (high Re) over the viscous forces then the flow is turbulent and Reynolds number effects need to be considered.

$$Re = \frac{\text{inetia forces}}{\text{viscous forces}} = \frac{\rho VD}{\mu} \quad (3.28)$$

Where V is the flow velocity, D is a characteristic linear dimension, ρ is the fluid density, μ is the dynamic viscosity.

The turbine performance characteristics is generally expressed in terms of non-dimensional parameters C_p and TSR, TSR does not actually represent flow velocity but is ratio of blade tip velocity and free flow velocity of water. Blades of the turbine are generally made from the airfoil sections whose drag and lift characteristics dependent on the operating flow velocity and Reynolds number.

3.5.5 Channel Geometry and Bed Forms

Rivers all around the world are characterized by the asymmetric channels, substrates and large meanders that respond differently to various stages of flooding. During the performance estimation of hydrokinetic turbine and project sites development the wide range of turbulence profile into the flow environment in the channel topography must be considered.

It has been shown that hydrokinetic turbines respond to a particular range of turbulence scales in the approaching flow. The cut-off frequency at which the turbine power is no longer affected by the turbulence is controlled by operational control of the turbine. This implies that the minimum turbulence scales capable of influencing the instantaneous turbine power are reduced as the tip speed ratio increases. Naturally, the tip speed ratio is determined by the mean cross sectional velocity and by the shape of the turbine blades. Based on these features, optimum working parameters are set to obtain maximum efficiency in the specified setting.

The previous researches have classified the five main flow regimes above the sand dunes are identified as.

a. **Maximum velocity-:** The maximum velocity is at the top of the dune above the crest where the minimum cross-sectional region is present.
b. **Shear layer-:** The shear layer is downstream of the dune crest and creates instability and high zone of turbulence intensity. This region can cause severe problem for the hydrokinetic turbine blades as it contains high concentration of suspended sediments and abrasive materials.
c. **Separation zone-:** This region is located downstream of the dune crest. This region creates a zone of high turbulence and often has recirculating, upstream velocities interacting with the lee side slopes of the dune. Separation zone extends downstream up to the reattachment point and is located typically at a horizontal distance of up to five times the bed forms heights.

d. Internal Boundary Layer-: A boundary layer develops along the low angle upstream side of the dune, downstream to the reattachment point.

e. Wake region-: It is located between the turbulent shear layer and the growing internal boundary layer is the wake region.

Table 3.1 Details of Hydrokinetic projects

Projects	Capacity(kW)	Turbine	Rotor Dia(m)	Velocity(m/s)	Depth of water(m)	Cut In speed(m/s)	Area(m^2)	System Efficiency (%)
RTT 2000	2000	Ducted Axial	25	3.1	<50	1	491	-
MCT	2500	Axial Propeller	18	3	<30	0.7	509 (2 rotors)	-
SMD hydro vision	1000	2 Blade Axial	18.5	2.3	-	0.7	537 (2 rotors)	-
UEK	400	Ducted Axial flow	4	3	-	1.54	38.6	-
UEK	10000	Ducted Axial Flow	-	3	-	-	-	-
Verdant Power rite	35.9	3 Bladed Axial flow	5	2.2	-	0.7	19.6	34
Kobold	150	3 Blade Darrieus	6	2.2	20	1	30	23
Mythos	500	3 Blade Darrieus	12	2.5	12	-	120	30
Roza Canal near Yakima	18	Savonius Turbine	-	-	1.8	-	-	-
Nenana, Alaska	25	Horizontal axis Darrieus	-	2.5	-	-	-	27
Eagle at Yukon river	61	Horizontal axis axial turbine	2	1.15	6.8	-	12.5(4 rotors)	40
Iguigig plant at Kvichak river	42	Horizontal axis axial turbine	1.5	1.39	2.4	-	21.2(2 rotors)	40
Whitestone at Tanana	593	Horizontal axis axial turbine	2	0.979	6.7	-	372(120 rotors)	40

3.6 PERFORMANCE OF HYDROKINETIC TURBINES UNDER SITE PARAMETERS

3.6.1 Effect of Free Surface on the Performance

The aim of the study is to understand the adverse effects which results from operating the hydrokinetic turbine near the free surface, or near the water-air interface between the atmosphere and the flowing river. The flow in the river near the turbine is characterized using the Froude number and Reynolds number. Distance between the tip of the blade and the initial undisturbed free surface level is turbine depth (d).

The turbine used in the investigation is propeller based turbine (HAHT). The proposed turbine has 2 blades, mean diameter 0.3745 m, solidity 0.83. Depths of 0.3048 m, 0.4572 m, 0.6096 m and 1.2192 m were used corresponding to the Froude number 1.31, 1.04, 0.92 and 0.71, respectively [16].

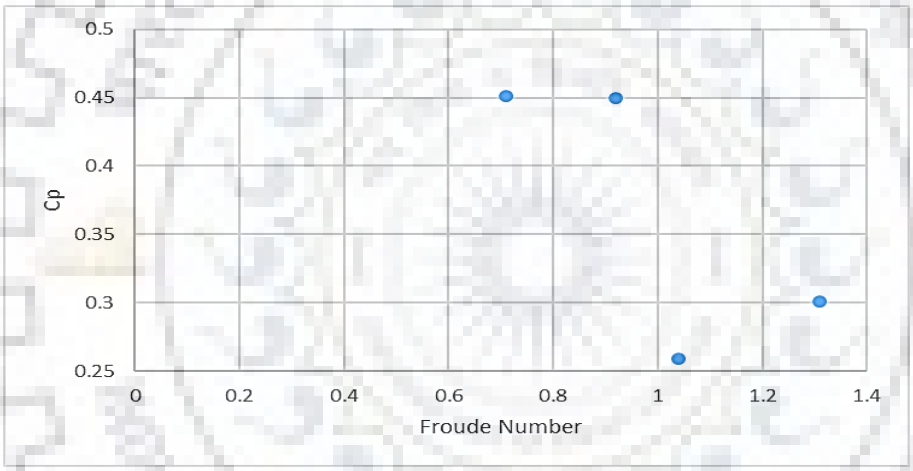

Fig 3.5 Power coefficient as a function of Froude number for axial flow hydrokinetic turbines [16]

Performance characteristics versus Froude number is shown in the Fig 3.5. The results showed that when the flow has become critical i.e. Froude number is equal to one than the performance of the turbine drops drastically. The power drop was found to be about 32 % as the Froude number is increased from 1.04 to 1.31. Plot in Fig 3.5 suggests that there is a substantial power drop near the critical Froude number (Fr=1).

In this study a vertical axis helical bladed turbine is used to see the effects of immersion level on the performance of the turbine. The parameters of the turbine used in the study are diameter of 300 mm, height of 300 mm, chord length of 120 mm and solidity of 0.38. The turbine was tested for velocities of 0.87 m/s, 0.85 m/s and 0.80 m/s

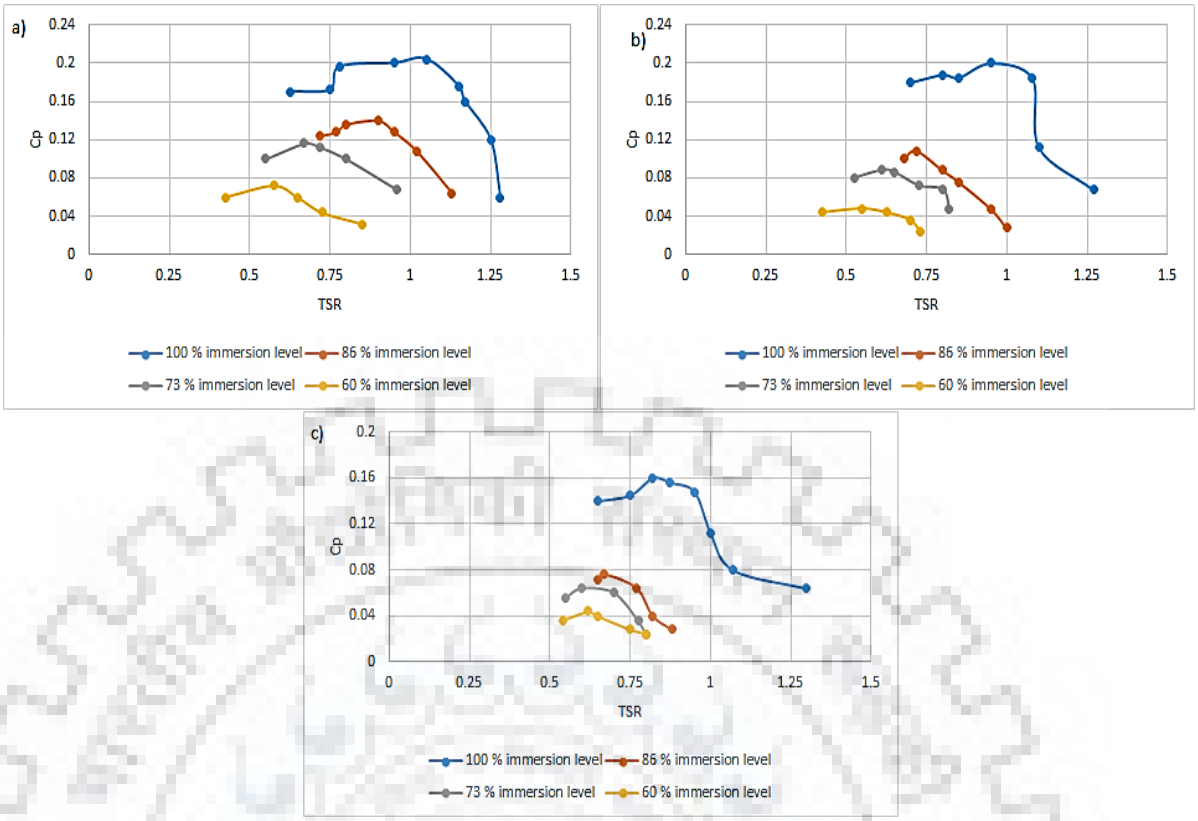

Fig. 3.6 Variation of the power coefficient with TSR of turbine at a) 0.87 m/s, b) 0.85 m/s and c) 0.80 m/s at different immergence level [26]

As shown in the Fig 3.6 it is evident that with the decrease in immersion level, the output power as well as power coefficient decreases and the maximum power coefficient shifts towards lower value of TSR. With the decrease in immersion level from 100% to 60%, the value of power coefficient drops with a difference of 64%, 70.3% and 73.1% respectively for the Fig 3.6 [a-c]. The reason for the decrease in the coefficient of power is that as the immersion level decreases the exposed area between the water and the turbine blades decreases. The water pressure increases as the depth below water level increase while at the free surface level the water pressure is equal to atmospheric pressure. The non-immersed part of the blade introduces air into the water leading to the flow separation caused by adverse pressure gradient in the case of partial immersion of turbines. Due to this flow separation there is a reduction in the contribution of the lift force to the net torque generation [26].

The prototype model used in this study is three bladed, 0.14 m radius, and horizontal axis hydrokinetic turbine. The water velocity at the inlet was 0.5 m/s. Tip clearance ratio was experimentally investigated in the range of 0.03 to 0.73 to predict the effect of free surface. Tip clearance ratio can be defined as the ratio of the depth of the tip of the blade of turbine from free surface to the total depth. For a tip clearance of 0.34 lowest turbine performance was observed. As the immersion depth is reduced the power coefficient increases until tip clearance ratio of

0.20 for all the cases of velocity except for the flow velocities less than 0.5 m/s. Therefore, flow with greater Froude number is more susceptible to boundary proximity effect. Fig 3.7 shows that with the increase in flow velocity resulted in improved performance coefficient. The performance of the turbine increases as the turbine is moved upwards from the channel bottom. Hence it is observed that if a turbine is in close proximity to the channel wall the flow field behind the turbine is affected and the performance is reduced. This trend continued until depth of immersion of turbine reached around 10 % of the channel depth (tip clearance ratio = 0.2) or 50 % of turbine radius.

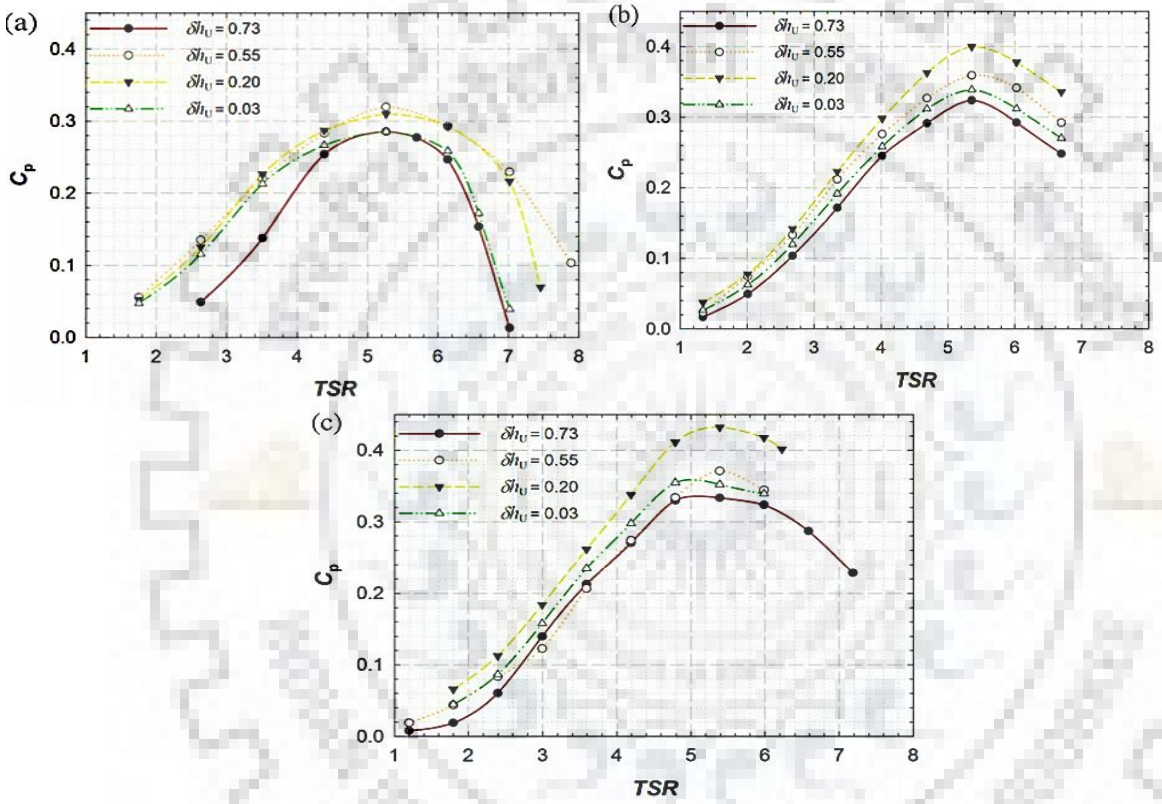

Fig. 3.7 Surface proximity effect on the turbine performance at different flow velocities a) U=0.5m/s b) 0.66 m/s c) 0.73 m/s [23]

From the Fig 3.7 it is observed that as the turbine is moved away from the bottom there is an increase in the performance of the turbine and this trend is continued till the turbine is raised to a tip clearance ratio of half the radius distance below the free surface after which the performance begins to decrease [23].

The turbine used for study is squirrel cage model vertical axis turbine with two blades. Turbine is 30 cm in diameter and 30 cm in height.

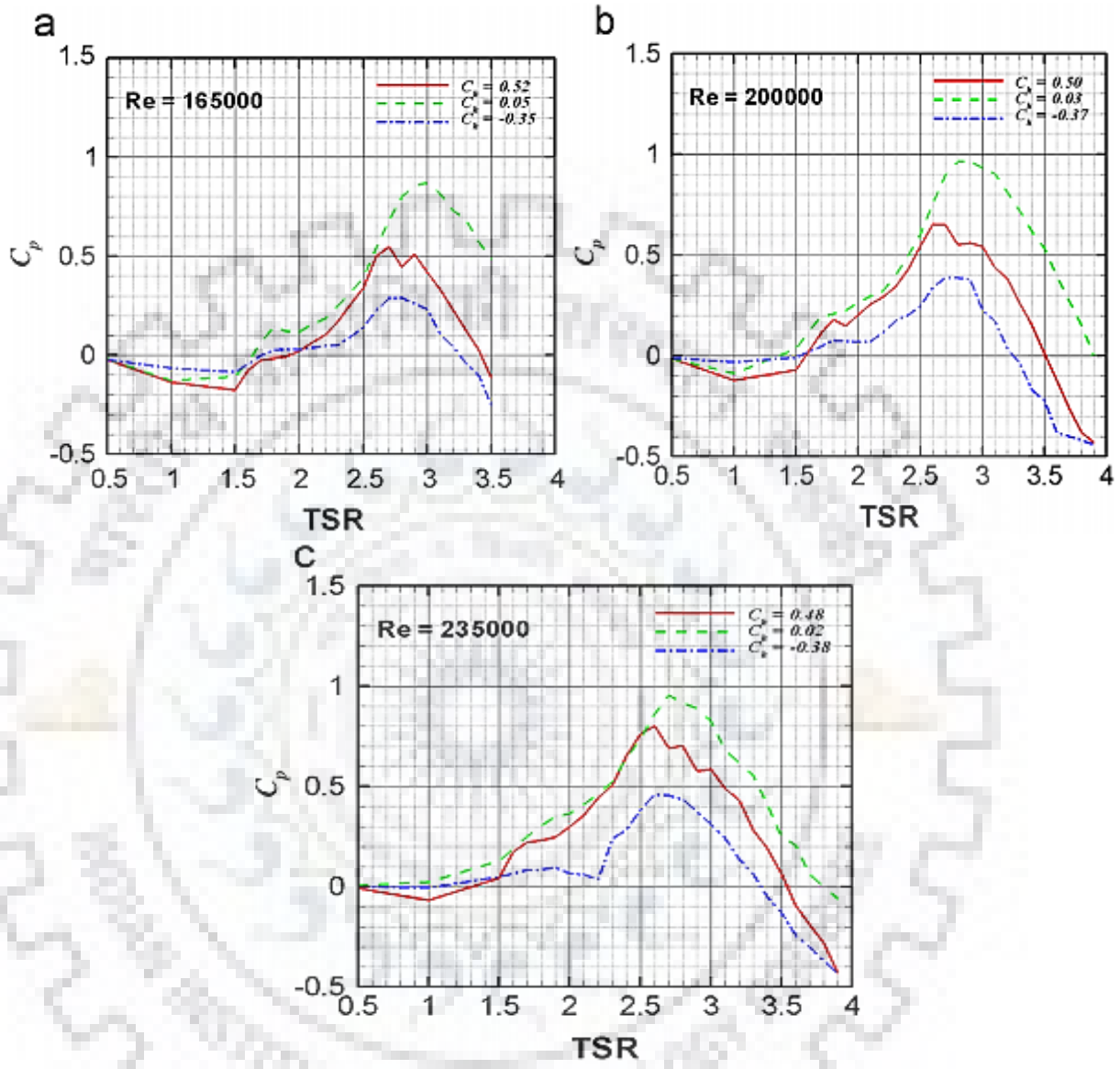

Fig. 3.8 Power coefficient variation with clearance height at Reynold number a) 1.65×10^5 b) 2.00×10^5 c) 2.35×10^5 [27]

The performance coefficient tends to decrease with increase in positive clearance coefficient as shown in the Fig. 3.8. The performance coefficient is maximum at around zero clearance coefficient. When the value of clearance coefficient is negative it means that the part of turbine blade is semi-submerged and part of it is exposed to air. Therefore the blade draws air in the water and there is a separation of water from blade which results in negative torque and power coefficient [27].

3.4.2 Effect of Flow Velocity on the Performance

The turbine used to study is Horizontal axis marine turbine. It is a 3 bladed turbine with 5 m diameter, the rated speed was set at 1.5 m/s and TSR of 3.5. The performance of turbine was determined at three different velocities 1.5 m/s, 3 m/s and 2.5 m/s.

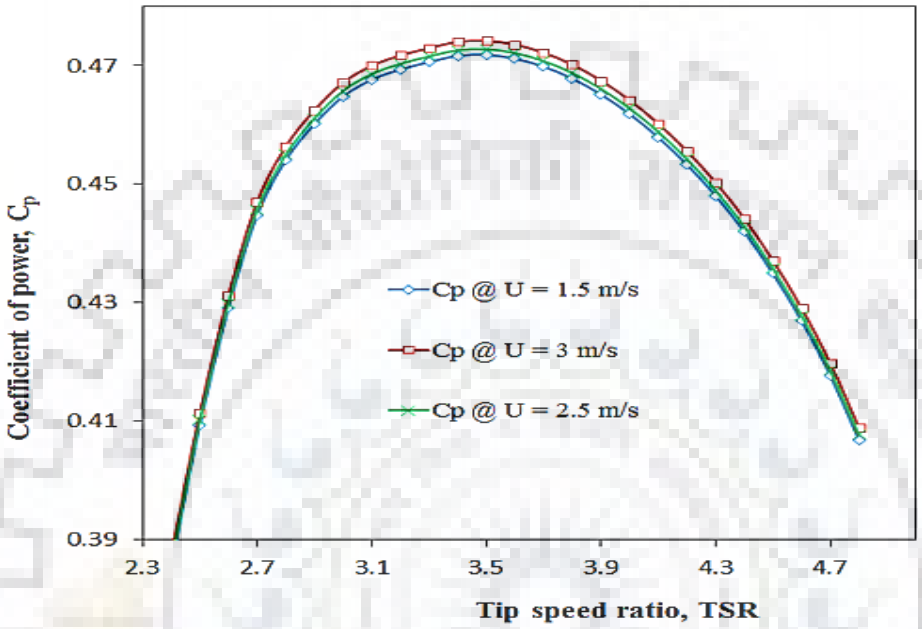

Fig. 3.9 Rotor performance at different operating conditions [47]

Fig 3.9 shows that turbine with larger velocity has a wider range of operating conditions than the turbines with low velocity[47].

The model prototype used for current study is a three bladed, 0.14 m radius, and constant chord 0.01676 m horizontal axis hydrokinetic turbine. At inlet a uniform flow velocity of 0.5 m/s was specified.

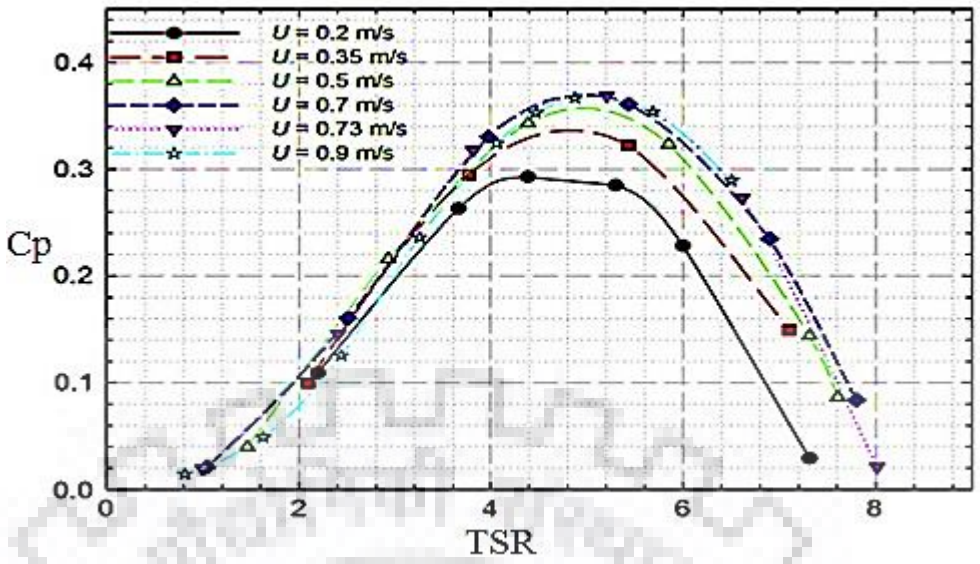

Fig. 3.10 Turbine performance characteristics with different flow velocities [23]

CFD simulations were carried out at the lab scale prototype in water channel sized fluid domain at flow velocities ranging from 0.1 m/s to 0.9 m/s. Fig 3.10 shows the variation of the performance characteristics with the flow velocity. As the velocity is increased by 0.1 m/s the turbine performance increases and the C_p versus TSR curve reaches higher maxima spreads over a wider TSR range. This trend in improvement of performance continued till the velocity reaches 0.7 m/s after which there was no significant change [23].

The turbine used in the study is Darrieus hydrokinetic turbine which consisted of four straight and fixed blades of length 400 mm with NACA 0015 cross section. The rotor diameter is of 600 mm and the blade chord length was 80 mm.

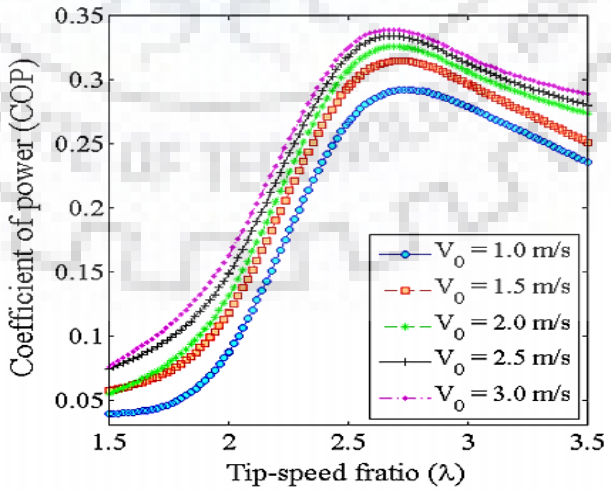

Fig. 3.11 Effect of free stream velocity on the turbines coefficient of power [48]

The maximum achievable performance coefficient increase with increasing free stream velocity. It is noticed that the rate of increase in performance coefficient decreases with the increase free stream velocity[48].

The influence of Reynolds number for a modified Savonius rotor (without shaft) for an overlap ratio of zero, aspect ratio of 0.7, blade arc angle of 124°, and blade shape factor of 0.2. As the Reynolds number increases the value of power coefficient increases. The change of the power coefficient was strongly effected in lower Tip speed Ratio [49].

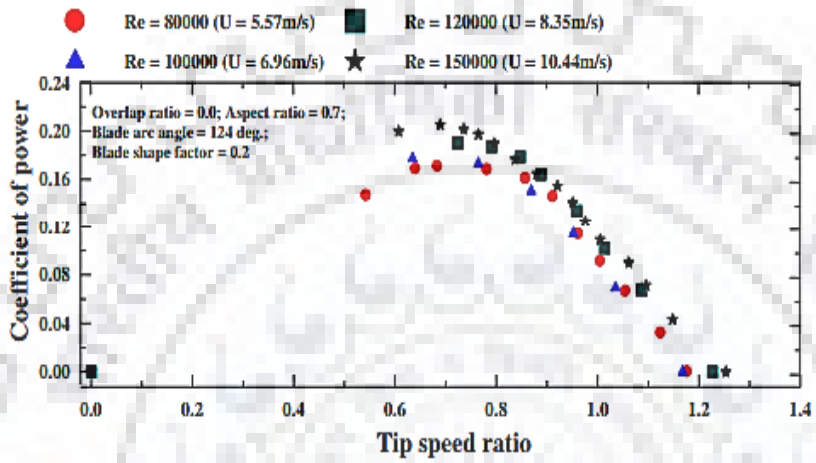

Fig. 3.12 Effect of the Reynolds number on the power coefficient [49]

3.4.3 Effects of Channel Blockage on the Performance

The study is performed on a 3 blade rotor with a TSR from 2.7-4.5 and Re = 1×10^7. The blockage ratio can be characterized as the ratio of the turbines frontal area to the cross sectional area of the channel. Three levels of refinement have been tested for a confined case at λ =3.5. For each of these cases the simulation was run until the drag and power coefficient had stabilized.

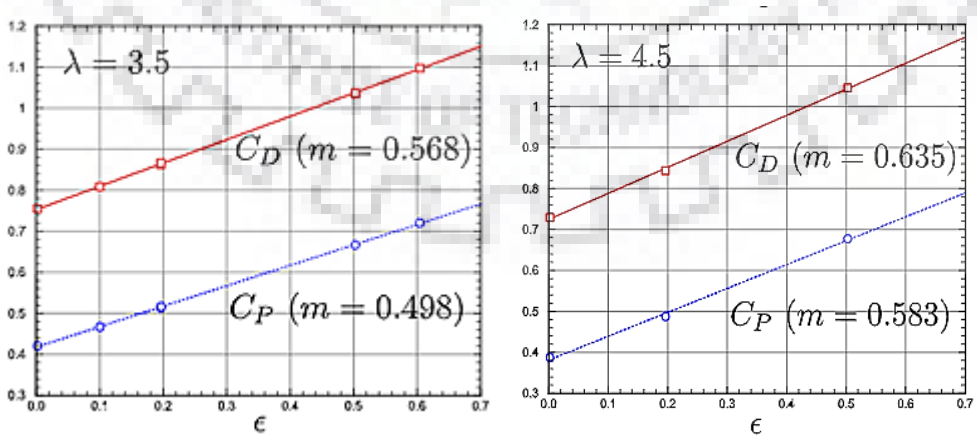

Fig. 3.13 Drag and power coefficients vs blockage ratio ε for axial flow hydrokinetic turbine [18].

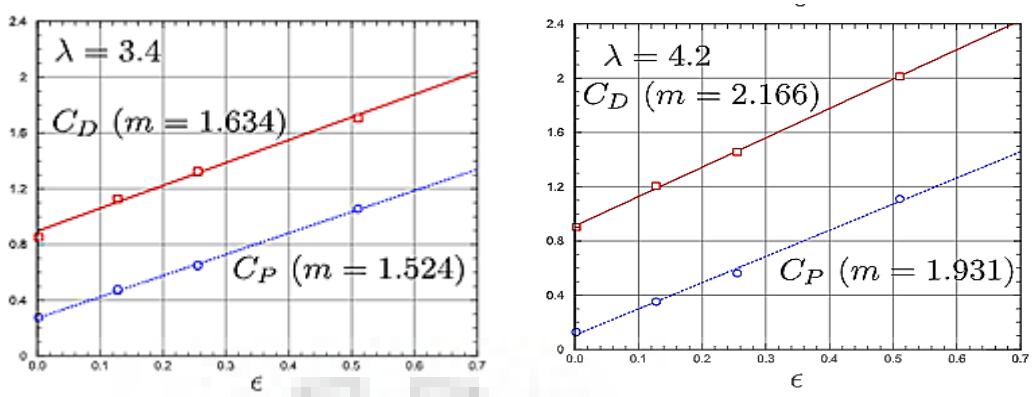

Fig. 3.14 Drag and power coefficients vs blockage ratio ε for cross flow hydrokinetic turbine [18].

In this study the blockage effect on two turbines (axial and cross flow) were investigated through numerical simulations. It is seen that for both the turbines, the drag and power coefficients increase essentially linearly with blockage. The graph shows linear behavior of the drag and power coefficients with blockage ratio. The slope of the plot is more for the TAHT then HAHT with same blockage ratio [18].

The model prototype used for current study is a three bladed, 140 mm radius, constant chord 16.76 mm horizontal axis hydrokinetic turbine. A uniform velocity of 0.5 m/s was specified at the inlet.

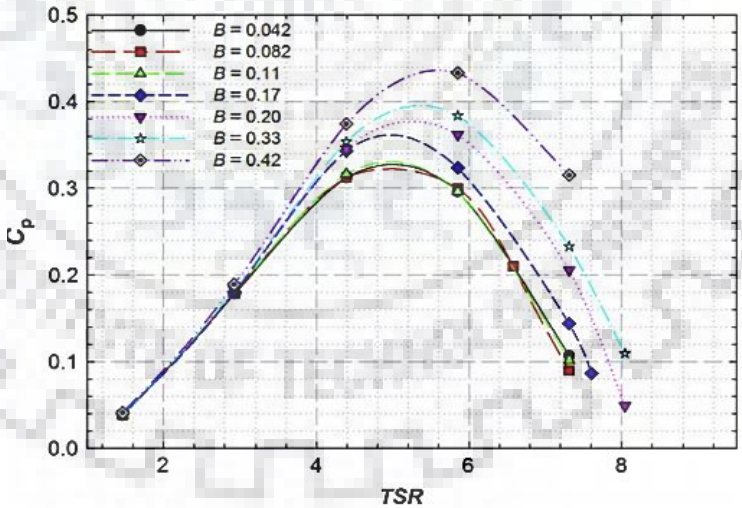

Fig. 3.15 Effect of the blockage ratio on the performance coefficient [23]

Fig. 3.15 shows variations in the performance of turbine with TSR at different blockage ratios.no variations were observed up to blockage ratio of 10 %, hence there was no requirement of blockage correction. As the blockage ratio increases beyond 10 % there was a consistent increase in the performance with up to an increase of 35 % in performance at 42 % blockage when compared to the unblocked case. The performance curve started divulging from each other

showing stronger influence of blockage as the TSR increases. The turbine torque increase at higher blockage ratios due to which the performance of the turbine improves [23].

3.4.4 Effect of Bed Forms and Channel Geometry on the Performance

The turbine used for the study is Savonius hydrokinetic turbine where the diameter of rotor is 90 mm, height of the vane is 100 mm and flow velocity is 0.46 m/s. The performance of Savonius type hydrokinetic turbines is calculated for five different hump heights. The output power of the hydrokinetic turbine can be increased if the flow striking the blades and the mass flow rate increases.

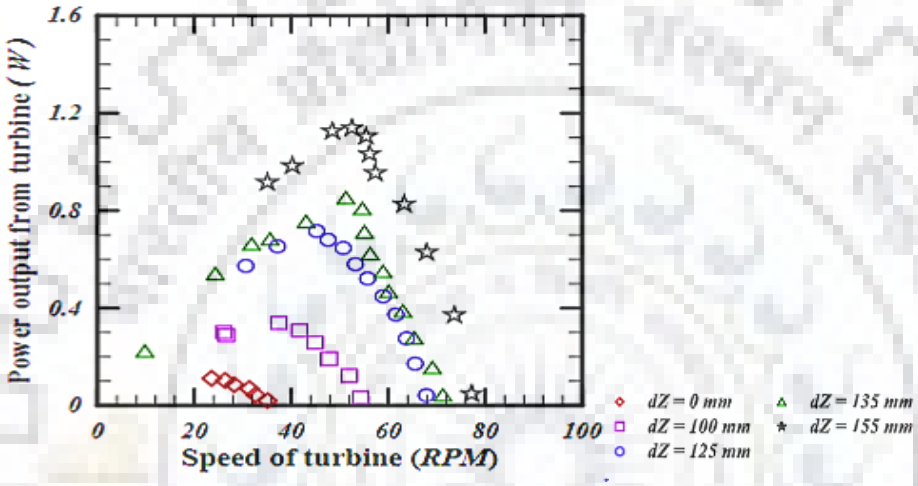

Fig. 3.16 Effect of the hump height on the power output [50]

From the Fig. 3.16 it is observed that there is significant increase in the output power by the use of a hump. It was also observed that the power coefficient is nearly same for all the cases [50].

The turbine used for the study is axial flow turbine with rotor diameter 150 mm and hub height of 130 mm. The experiment was conducted in clear water condition to assess the impacts of local scour on single and two turbines installation. The turbine voltage output value were simultaneously obtained with the measurements of bed elevations. The experiments was conducted in a mobile bed of 1.8 mm coarse sands with migrating bed forms. The presence of the additional turbine upstream as well as passage of local bed forms effected mean and fluctuating voltage of the primary turbine. The presence of the bed forms increased the range of voltage fluctuations 2-3 times more than that during clear water experiment. The greatest influence on mean power was the proximity to the turbine rotor plane to the peak of the dune. The power increases as the velocity increases due to the decrease in the cross sectional area above the dunes [19].

3.7 SELECTION OF SAVONIUS HYDROKINETIC TURBINE FOR NUMERICAL ANALYSIS

The hydrokinetic energy is harnessed by hydrokinetic devices which are classified in two categories: axial and cross flow hydrokinetic turbines. Axial flow turbines have better efficiency over cross flow hydrokinetic turbines however there manufacturing and transportation cost is high as they have complicated and fragile design structure. Furthermore these turbine are suitable for energy extraction from the applications having high depth viz. Ocean.

On the other hand cross flow hydrokinetic turbines possesses less efficiency compared to axial flow hydrokinetic devices but their applicability in terms of sites is more. Cross flow turbines are less complex and have good debris handling capabilities. These turbines can work in horizontal as well as in vertical orientation of rotor shafts and can capture the potential of hydrokinetic energy in more effective manner. The number of components in cross flow turbines is relatively less than the axial flow turbines. These can be operated close to ground levels and have very low noise. The cost of power generation of cross flow turbines is less than the axial flow turbines. Cross flow turbines are more suitable for river applications. Savonius is the common cross flow hydrokinetic turbine and the effects of site parameters would be applicable for all kind of cross flow hydrokinetic turbines viz. Darrieus, Gorlov, Squirrel cage. Savonius turbine is selected due to its easy construction and maintenance during operation. It works on drag force principle and possess good starting characteristics. Further the installation of Savonius turbine would be helpful for the deployment of cross flow hydrokinetic turbine working under different operating conditions.

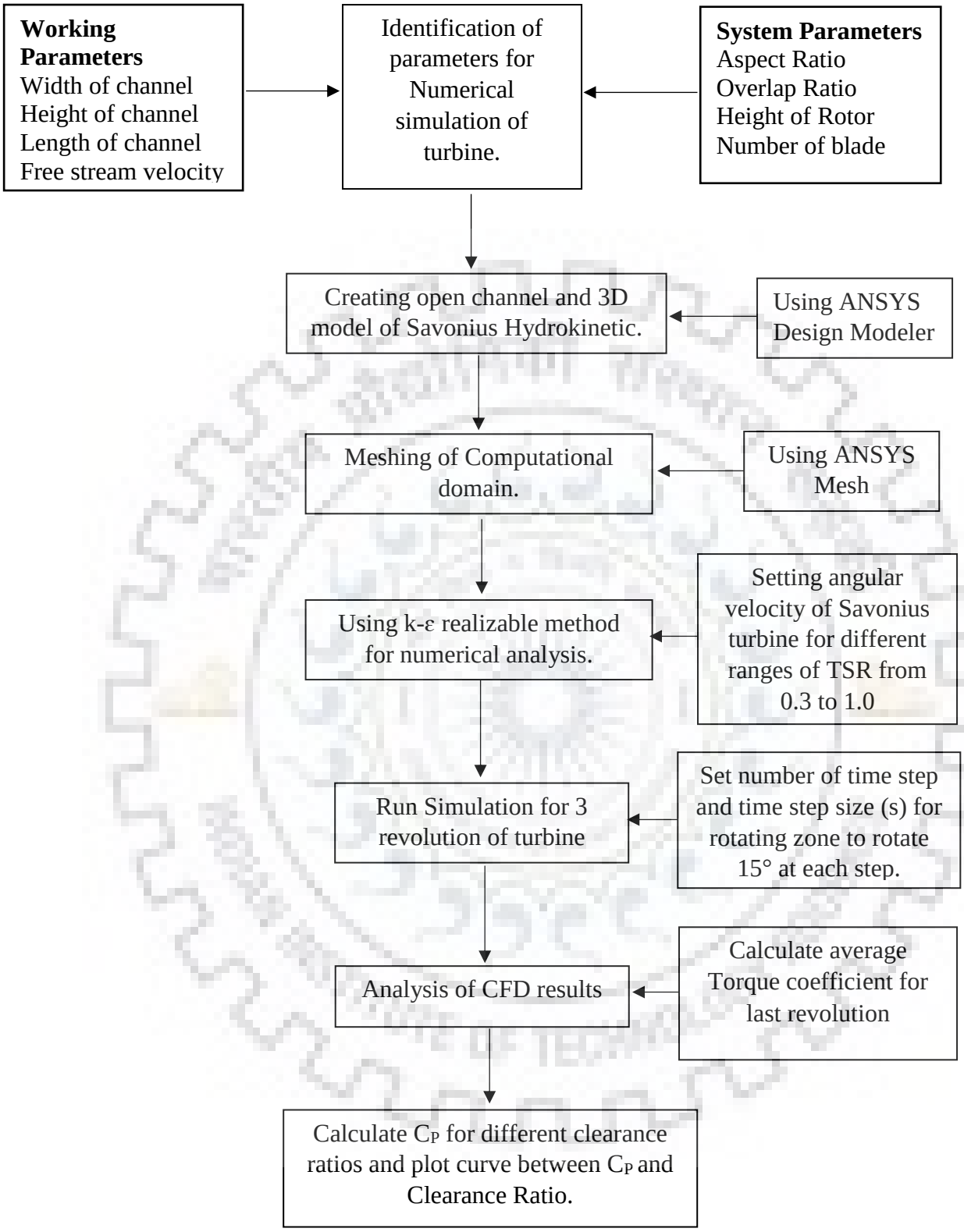

Fig. 3.17 Methodology adapted for the current numerical analysis.

CHAPTER 4

PARAMETRIC ANALYSIS OF SAVONIUS HYDROKINETIC TURBINE USING NUMERICAL (CFD) SIMULATION

4.1 GENERAL

A parametric study of Savonius Hydrokinetic (Cross flow) Turbine is carried out by using the k-epsilon realizable model in its unsteady form. The effect of installing the hydrokinetic turbine at four different heights while keeping other parameters were kept fixed viz. number of blades, blockage ratio, TSR, Flow velocity. The effect of different TSR is also calculated at various depths. The power coefficient of the turbine is evaluated at different tip speed ratios and height of installation of turbine from the channel bed.

4.2 DESIGN PARAMETERS OF SAVONIUS HYDROKINETIC TURBINE

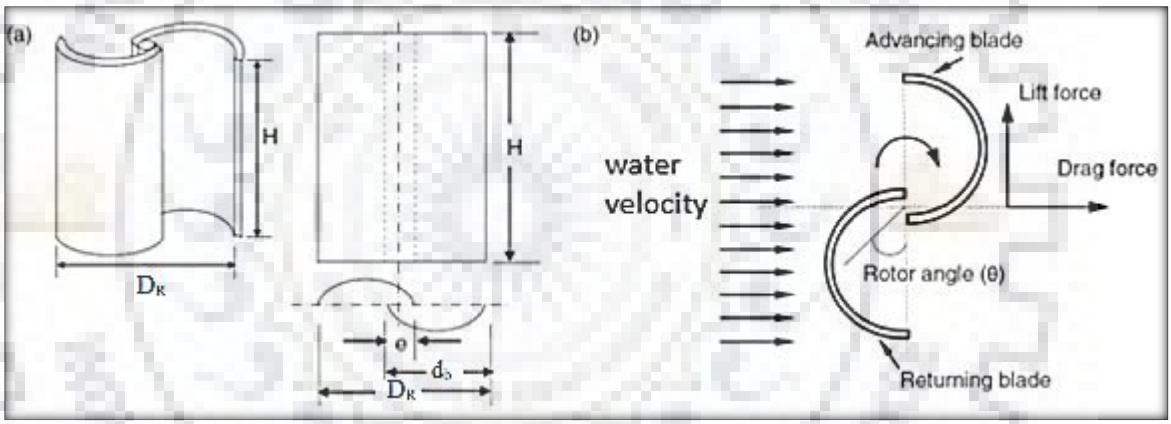

Fig 4.1 a) A typical two bladed Savonius turbine b) forces acting on the rotor

The design of Savonius hydrokinetic turbine consists of two half vertical cylinders shown in the Fig. 4.1.The rotor height is denoted by 'H' and rotor diameter is denoted by 'D_R'. Aspect ratio is defined as the ratio between rotor height (H) and rotor diameter (D_R). Other parameter that affects the performance of Savonius rotor is the overlap ratio (G) which is expressed as $G=e/d_b$, where e is the overlap and d_b is the blade diameter. Advancing blade make a drag force from free flow while returning blade develops a returned force from the opposite direction outflow through the gap (overlap) resulting in pair of couple force that is able to generate torque and power.

Table 4.1 Geometrical parameters of Savonius Hydrokinetic turbine

Rotor Parameters	**Value**
Number of blades	2
Aspect Ratio(H/D_R)	1
Diameter of Rotor(D_R)	250 mm
Diameter of blade(d_B)	144 mm
Overlap distance	38 mm
Overlap ratio	0.152

Table 4.2 Parameters of channel

Channel Parameter	**Value**
Length of channel	1500 mm
Width of channel	700 mm
Height of channel	600 mm
Distance of Turbine installation from inlet	500 mm

4.3 DESIGNING OF 3-D TURBINE MODEL IN DESIGN MODULAR

Present numerical (CFD) analysis is carried out on the commercially available simulation software ANSYS. ANSYS provides a platform to carry out the simulation in a step by step process starting from the 3D model design, mesh generation, setting the CFX solver to the post CFD analysis.

A 3-D design is created in the design modular of ANSYS. It consists two parts i.e., channel and rotating region (turbine rotor) shown in Fig. 4.2 and isometric view of both the turbine and channel are shown in Fig. 4.3.

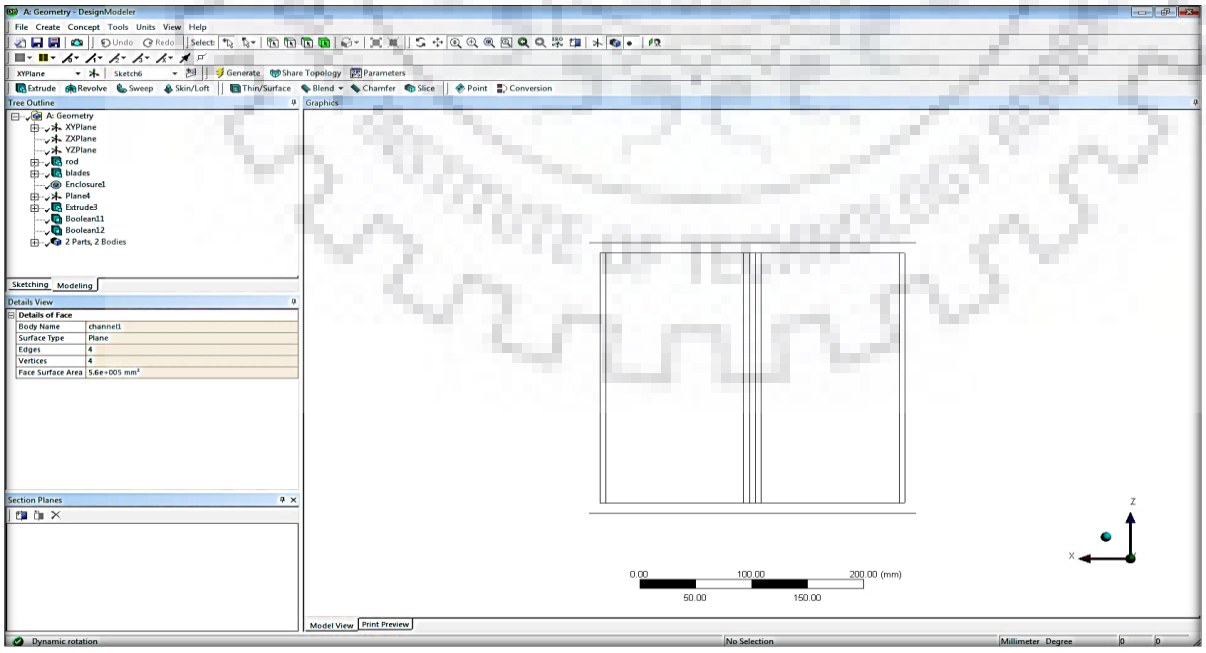

Fig 4.2 Representation of the Savonius hydrokinetic turbine in front view

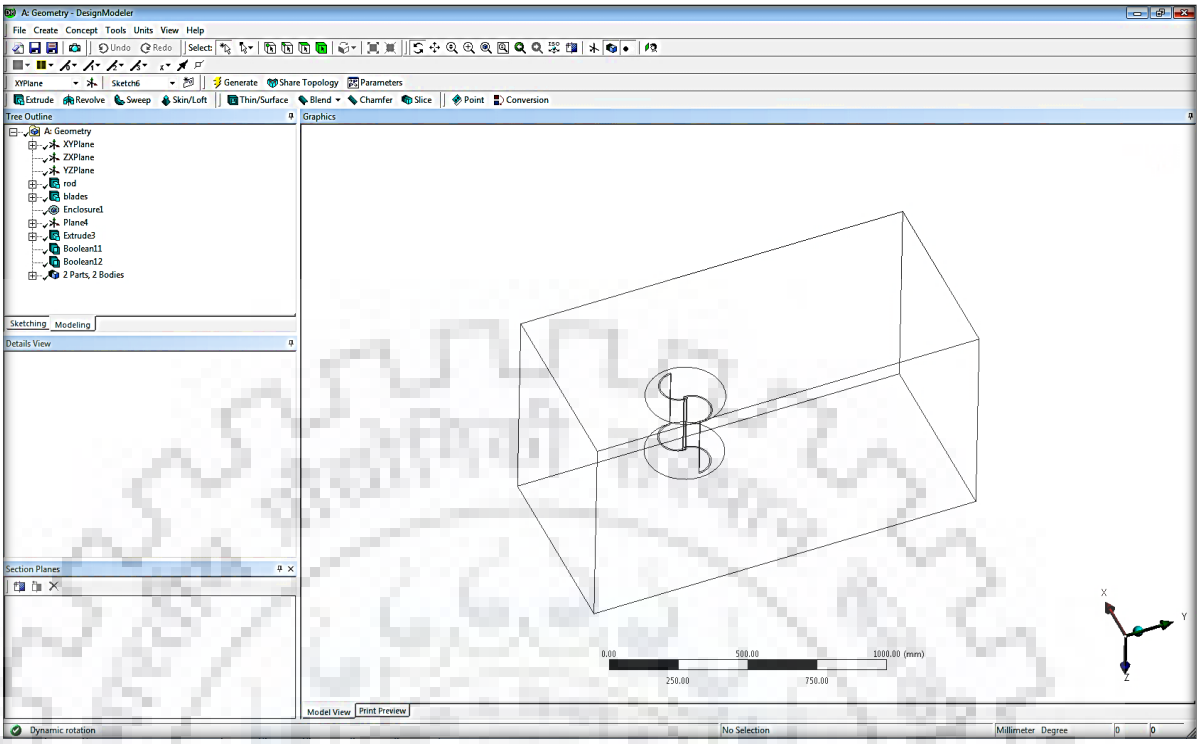

Fig. 4.3 Isometric representation of Savonius Turbine in the channel

4.4 MESH GENERATION AND STRATEGY FOR CALCULATION

The mesh is the most important part of the CFD simulation for the analysis purposes. It has to be fine enough so that each important physical phenomenon can be simulated and captured, but also coarse enough that the calculations are affordable.

The concept is to have a mesh that is adaptable to the various configurations. Mesh interface is used between the calculation domain i.e., the enclosure and the rotating turbine. The meshing of the complete system is shown in Fig. 4.4. Further detailed meshing of turbine rotor is shown in Fig. 4.5.

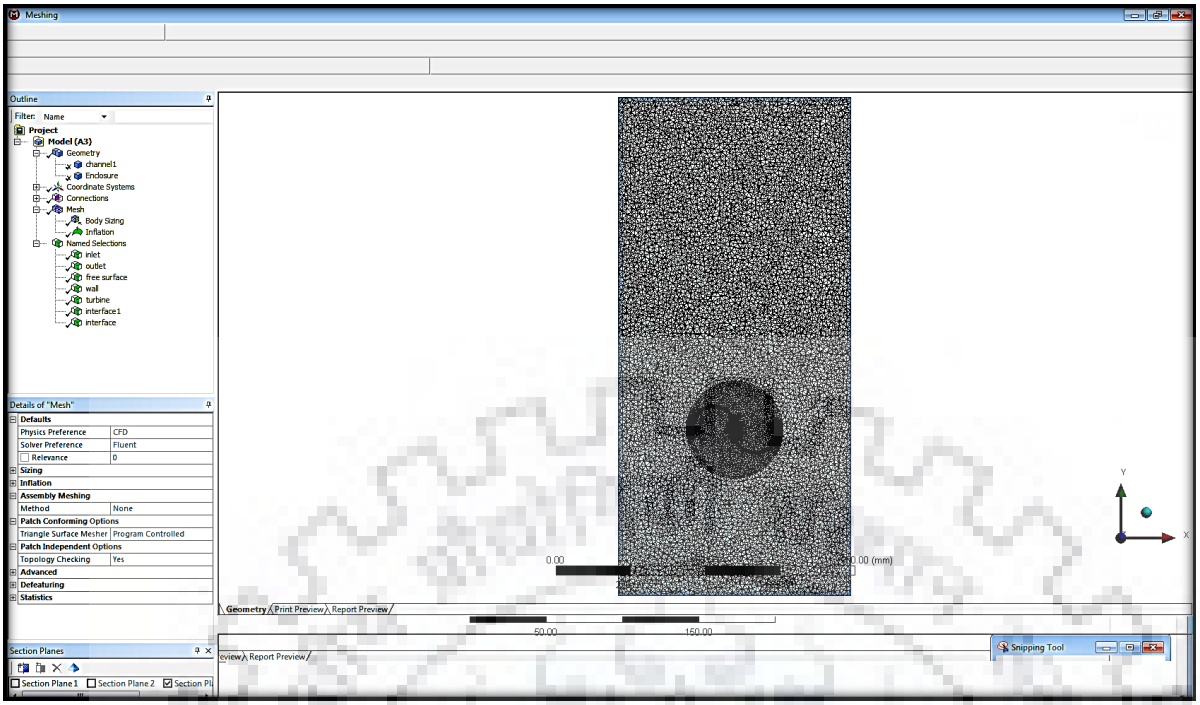

Fig. 4.4 Meshing of complete channel and turbine rotor system

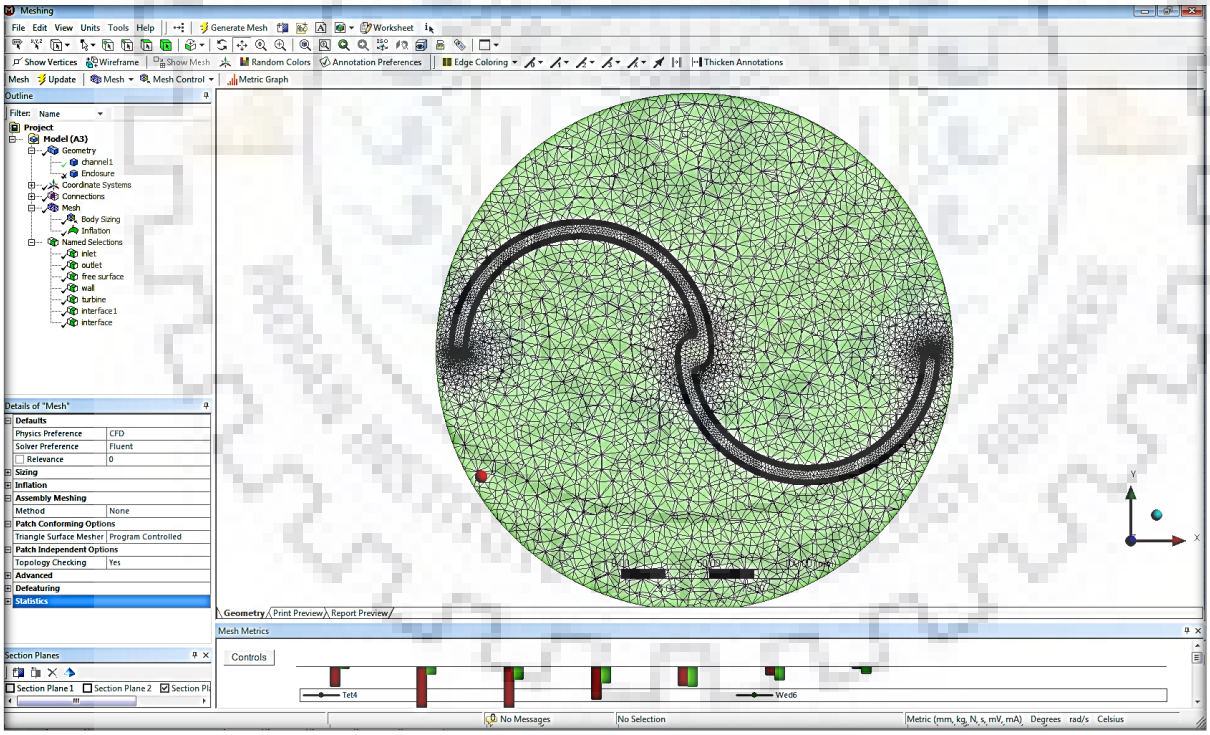

Fig.4.5 Detailed meshing of turbine rotor

For mesh generation all triangles method is used and inflation is applied to have better accuracy of flow over the blades as shown in Fig. 4.6 and inflation is applied over the top and bottom boundary of the enclosure. Further edge sizing and face sizing of different components is being done by using different element sizes.

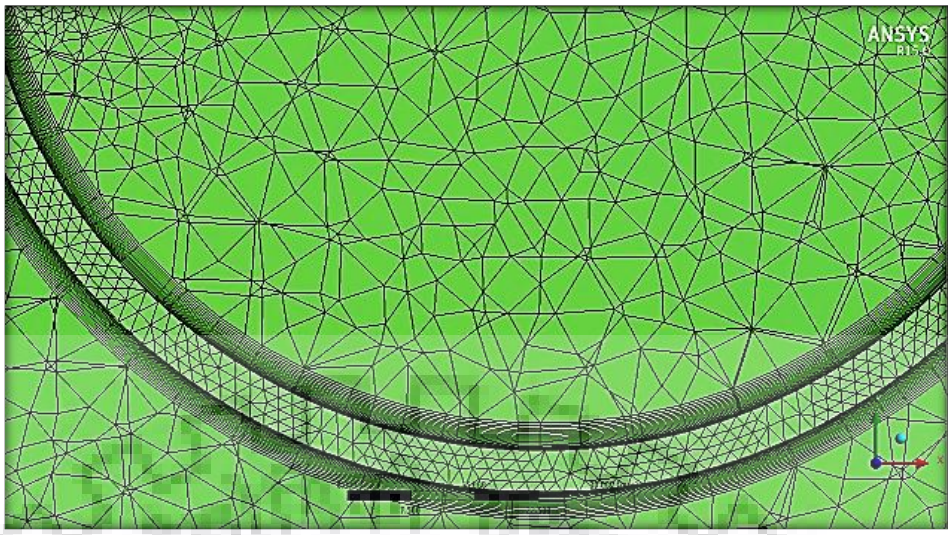

Fig. 4.6 Detailed meshing of profile by using inflation

The mesh zones containing the profile of the blades are the same between every simulation in this work, ensuring that the boundary layer behavior is similar for the different cases. Further the meshed system have 1434780 nodes and 5034632 elements having skewness of 0.84919 (which is under the permissible limits).

Boundary conditions typically consists of two planes of symmetry (top and bottom), a uniform inlet velocity on the boundary with magnitude 1.5 m/s and outflow on the outlet boundary is absolute atmospheric pressure. Turbulent conditions at the inlet boundary having 5% turbulent intensity and turbulent viscosity ratio of 10 using intensity and viscosity ratio specification method. A 3D mesh is created and time step is expressed on a per cycle basis. 72 time steps, with maximum iterations of 100 per time step and different step sizes are used for different calculations. As for different calculations, different angular speed is taken in order to have variable tip speed ratios (TSR).

4.5 SIMULATION METHOD

4.5.1 Numerical Method

In the present study, the numerical simulations are performed with the commercial ANSYS CFX. The simulation is conducted with the SIMPLE (Semi Implicit Method for Pressure-Linked Equations) pressure velocity coupling with least square cell based algorithm. Standard scheme is for pressure along with the second order upwind scheme was utilized for turbulent kinetic energy (*k*), momentum and specific dissipation rate (w) formulation. A second order implicit scheme is also used for transient formulations. Absolute reference frame is used for each variable (turbulence kinetic energy, velocity components, and specific dissipation rate).

4.5.2 Turbulence Modelling

Although large-eddy simulation (LES) model attract much interest because of rather expensive computing times there use is restricted. The standard k–ε turbulence model that has been commonly used has some shortcomings when it is applied to the simulation of flow separation and impingement. Renormalization group (RNG) k– ε turbulence model is an improvement over the standard k– ε turbulence model. Orszag and Yakhot applied the RNG k–ε method to the Navier–Stokes equations and the equations of passive scalar to evaluate turbulence statistics. The primary concept of the RNG technique is to systematically remove small turbulence scales by representing their impacts in terms of larger movements and altered viscosity.

There are many turbulence models, among which the most frequently used for engineering applications are Spalart- Allmaras, k- ε and k-ω. K-ω SST (Shear Stress transport) model is the combination of the k- ε and k-ω. While the other two models are used to solve the Reynolds-averaged Navier Strokes equations up to the wall whereas the k- ε uses a wall function to resolve the boundary. In most cases where the boundary layer remains attached to the body, k-ε gives result similar to other models while using a coarser mesh near the walls, reducing the time required to complete the calculation. However, in the case of boundary layer separation, a wall function is not suitable for capturing all the physical phenomenon occurring in the important part of the flow field, and result is often off from reality. Resolving the Navier-Stokes equations up to the walls is costly mesh-wise, but this kind of turbulence modelling has led to better agreement with experimental data, especially in oscillating airfoils and dynamic stall problems, or more generally in cases with boundary layer separation. Considering the advantages in terms of simulation reliability and relative low run time for full simulation, realizable k- ε standard wall fin has been considered to carry out the current parametric analysis.

The transport equations for the k and ε in the realizable k- ε model are given below.

$$\frac{\partial}{\partial t}(\rho k) + \frac{\partial}{\partial x_j}(\rho k u_j) = \frac{\partial}{\partial x_j}\left[\left(\mu + \frac{\mu_t}{\sigma_k}\right)\frac{\partial k}{\partial x_j}\right] + G_k + G_b - \rho\varepsilon - Y_M + S_k \quad (4.1)$$

$$\frac{\partial}{\partial t}(\rho \varepsilon) + \frac{\partial}{\partial x_j}(\rho \varepsilon u_j) = \frac{\partial}{\partial x_j}\left[\left(\mu + \frac{\mu_t}{\sigma_\varepsilon}\right)\frac{\partial \varepsilon}{\partial x_j}\right] + \rho C_1 S_\varepsilon + \rho C_2 \frac{\varepsilon^2}{k+\sqrt{v\varepsilon}} + C_{1\varepsilon}\frac{\varepsilon}{k} C_3 G_b + S_\varepsilon \quad (4.2)$$

Where;

$$C_1 = \max\left[0.43, \frac{\eta}{\eta+5}\right],\ \eta = S\frac{k}{\varepsilon} \text{ and } S = \sqrt{2 S_{ij} S_{ij}} \quad (4.3)$$

For the case of standard k- ε model C_μ is constant whereas for realizable k- ε model it varies and can be calculated using following equation 4.4

$$C_\mu = \frac{1}{A_0 + A_s \frac{kU^*}{\varepsilon}} \quad (4.4)$$

Where;

$$U^* = \sqrt{S_{ij}S_{ij} + \Omega_{ij}\Omega_{ij}} \quad (4.5)$$

$$\Omega_{ij} = \Omega_{ij} - 2\varepsilon_{ijk}\omega_k \quad (4.6)$$

Where;

ε is the dissipation rate of the turbulent kinetic energy

ρ is the fluid density

k is the turbulent kinetic energy

x_j is the Cartesian coordinate,

u_j is the velocity components

t is the time

μ is the viscosity

σ_k is the constant of the standard k-ε turbulence model

μ_t is the turbulent viscosity

G_b is the generation of turbulence kinetic energy due to buoyancy

G_k represents the generation of turbulence kinetic energy due to the mean velocity gradients

U_{ij} is the mean rate-of-rotation tensor viewed in a rotating reference frame with the angular velocity ω_k

Y_M is the effect of the changing dilatation in compressible turbulence to the overall dissipation rate.

S is the assumed source terms

The summary of the solver settings is presented in Table 4.3

Table 4.3 Setting of the solver

S.No.	Settings	Parameters
1.	Solver	Type: Pressure Based Velocity formulation: Absolute
2.	Viscous Model	Realizable k- ε
3.	Material	Water (Liquid)
4.	Boundary Conditions	Turbine: Moving wall, No slip Side and bottom surface: Stationary wall, No Slip Top Surface: Free slip wall Inlet: Velocity inlet Outlet: Absolute pressure 1 atm
5.	Solutions Method	Pressure velocity coupling: SIMPLE
6.	Spatial Discretization	Gradient: Least Squares Cell based Pressure: Standard Momentum: 2^{nd} Order Upwind Turbulence Kinetic Energy: 2^{nd} Order Upwind Specific Dissipation: 2^{nd} Order Upwind Transient Formulation: 2^{nd} Order Implicit
7.	Solution Initialization	Standard Reference Frame: Absolute

4.5.3 Velocity and Pressure Field Contours

The velocity streamlines for the around the turbine rotor in the channel is shown in Fig. 4.7 Streamlines are the imaginary lines which are drawn tangential to the velocity vector at every point in the flow at any given instant. Velocity streamlines help in understanding the flow around the rotor. In velocity streamlines the color of the line represent the magnitude of the flow while vector direction represents flow direction. A high turbulence area is seen just behind the rotor of the turbine where the streamlines are non-uniform. The tip of the advancing blade acts as the stagnation point where the pressure is found to be maximum and the fluid velocity at this point is zero and all kinetic energy has been converted into pressure energy. After passing through the Savonius rotor the pressure starts increasing and the flow experiences an adverse pressure gradient. There is separation of flow behind the rotor and a high turbulence area is formed due to the adverse pressure gradient.

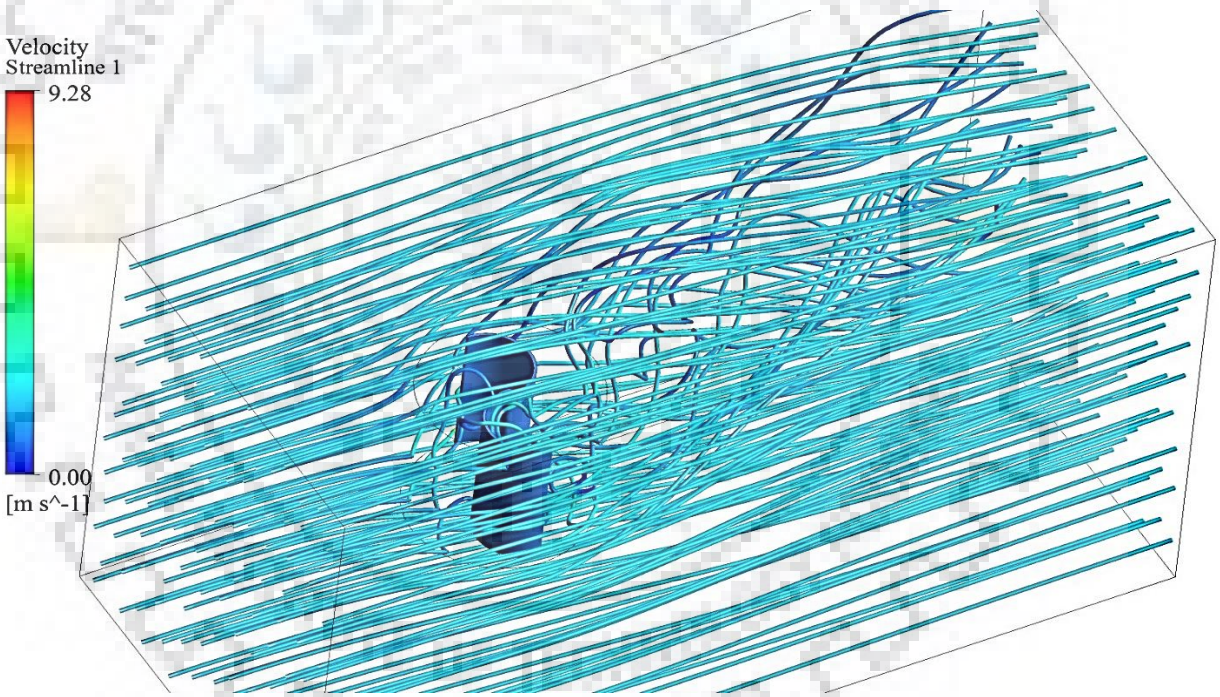

Fig. 4.7 Velocity Streamlines around the complete channel and channel system

Pressure contours are used to predict the pressure variations in the various regions near the blades within the flow domain. The maximum and minimum pressure contours are represented by the color. At the inlet of the channel the pressure is found to be uniform. High pressure is found at the upstream side of the concave side of the advancing blade and convex side of the returning blade. Lower pressure is developed on the downstream side (the concave side of the returning blade and the convex side of advancing blade). Therefore the two pressure regions i.e.

the higher and the lower are found near the flow domain thus creating a pressure drop across the rotor hence facilitating power extraction by the Savonius hydrokinetic turbine from the flowing water in the channel. The pressure contours of the simulation is shown in Fig. 4.8.

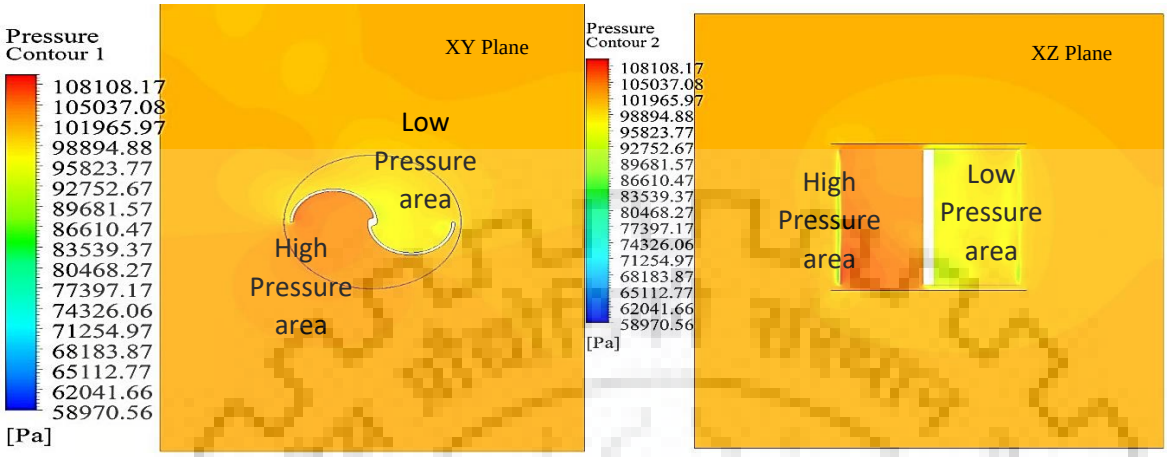

Fig. 4.8 Pressure contours of flow around the turbine rotor in XY and XZ planes

Velocity contours plots predict velocity differences within the flow domain in different regions near the blades. In the Fig. 4.9 High speed zone has been found at the tip of the blade. The low speed zone was observed behind the rotor blades due to the rotation of the turbine.

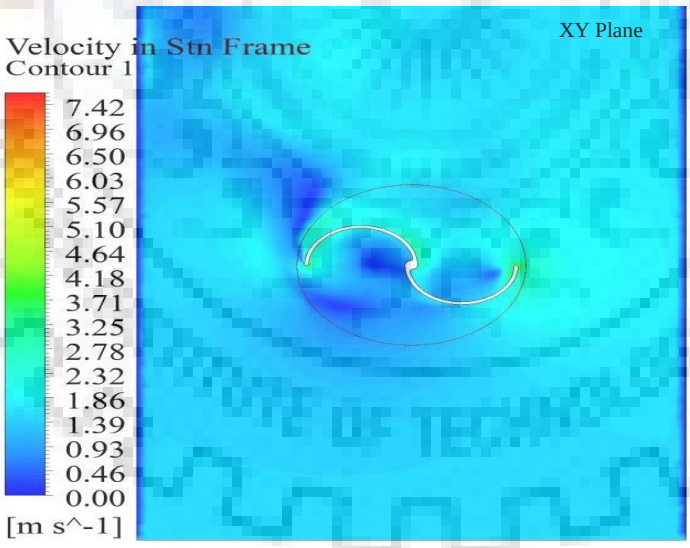

Fig. 4.9 Velocity field contours of flow around turbine rotor

4.6 CFD RESULTS ANALYSIS AND DISCUSSIONS

Numerical analysis of the Savonius hydrokinetic turbine at different Clearance Ratios has been done and after running the simulation, data for the torque is obtained for different tip speed ratios. From these results power coefficient was calculated manually and performance curves were plotted further.

A non-dimensional parameter called clearance ratio is defined to compare the results of the CFD analysis. Clearance ratio is defined as the ratio of height of installation for the turbine form the channel bottom to total depth of the channel.

$$\text{Clearance Ratio (CR)} = \frac{\text{Height of turbine installation from channel bottom (d)}}{\text{Total depth of the channel (D)}} \quad (4.1)$$

The data pertaining to the performance coefficient of turbine at different level of heights from bottom of channel and at different TSR is given in Table 4.4. The side view of the turbine in the channel is shown in Fig. 4.10.

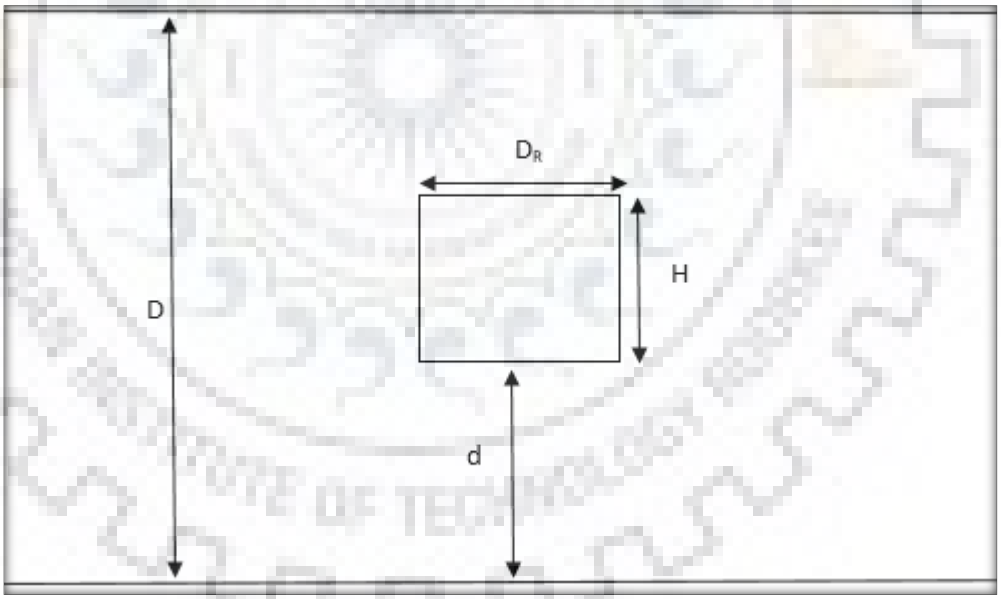

Fig 4.10 Schematic of the Turbine and the channel in side view

Table 4.4 Numerical Data of the CFD analysis at various depths of installation in tabulated form

Velocity(m/s)	TSR	d(mm)	CR(d/D)	RPM	P_{in}(W)	Avg Torque (N/m)	P_{out} (W)	C_P	C_T
1.5	0.3	500	0.83	34.39	105.26	3.52	12.67	0.1204	0.4013
		305	0.51			3.91	14.08	0.1337	0.4458
		240	0.40			3.76	13.54	0.1286	0.4287
		153	0.25			3.87	13.90	0.1320	0.4401
	0.5	500	0.83	57.32		4.25	25.50	0.2423	0.4845
		305	0.51			4.41	26.46	0.2514	0.5028
		240	0.40			4.35	26.10	0.2480	0.4959
		153	0.25			4.40	26.40	0.2508	0.5016
	0.8	500	0.83	91.72		3.87	37.15	0.3530	0.4412
		305	0.51			4.03	38.69	0.3676	0.4594
		240	0.40			3.97	38.11	0.3621	0.4526
		153	0.25			4.00	38.40	0.3648	0.4560
	1.0	500	0.83	114.65		2.85	34.20	0.3249	0.3249
		305	0.51			3.04	36.48	0.3466	0.3466
		240	0.40			2.97	35.64	0.3386	0.3386
		153	0.25			3.02	36.24	0.3442	0.3442

4.6.1 Relationship between Performance Coefficient and Clearance Ratio

The relation between Performance Coefficient and Clearance Ratio is shown in Fig. 4.11. Power coefficient for different clearance ratio has been plotted for various TSR. The value of power coefficient is maximum at a clearance ratio of 0.51. The peak performance is attained at clearance ratio of 0.51 and the value of C_p at 0.3 TSR is 0.1357. Performance coefficient at 0.3 TSR increases by 1.33 % when installed from the clearance ratio of 0.83 to 0.51. The C_p for the same change in the clearance ratio i.e. 0.83 to 0.51 changes by 0.91% at 0.5, 1.46 % at 0.8 TSR and 2.28 % at 1.0 TSR.

At a clearance ratio 0.25 the value of C_P is relatively higher than at the clearance ratio of 0.83 and 0.40 The reason for the increase in the performance coefficient can be contributed to the turbulence intesity which decreases drastically very close to the channel bed, hence the interaction of fluid with the blades of the turbine is smooth. At a clearance ratio of 0.40 the value of C_P decreases as the turbulence intensity increases and turbulence intesity reaches its maximum at a certain depth and then it starts decreasing gradually. The value of C_P is maximum at a clearance ratio of 0.51. An important finding here is that the value of C_P decreases as the turbine is installed near the free surface this is due to the induction of air bubbles from the free surface into the water which decreases the performance of the turbine as it separates the water from the blade surface.

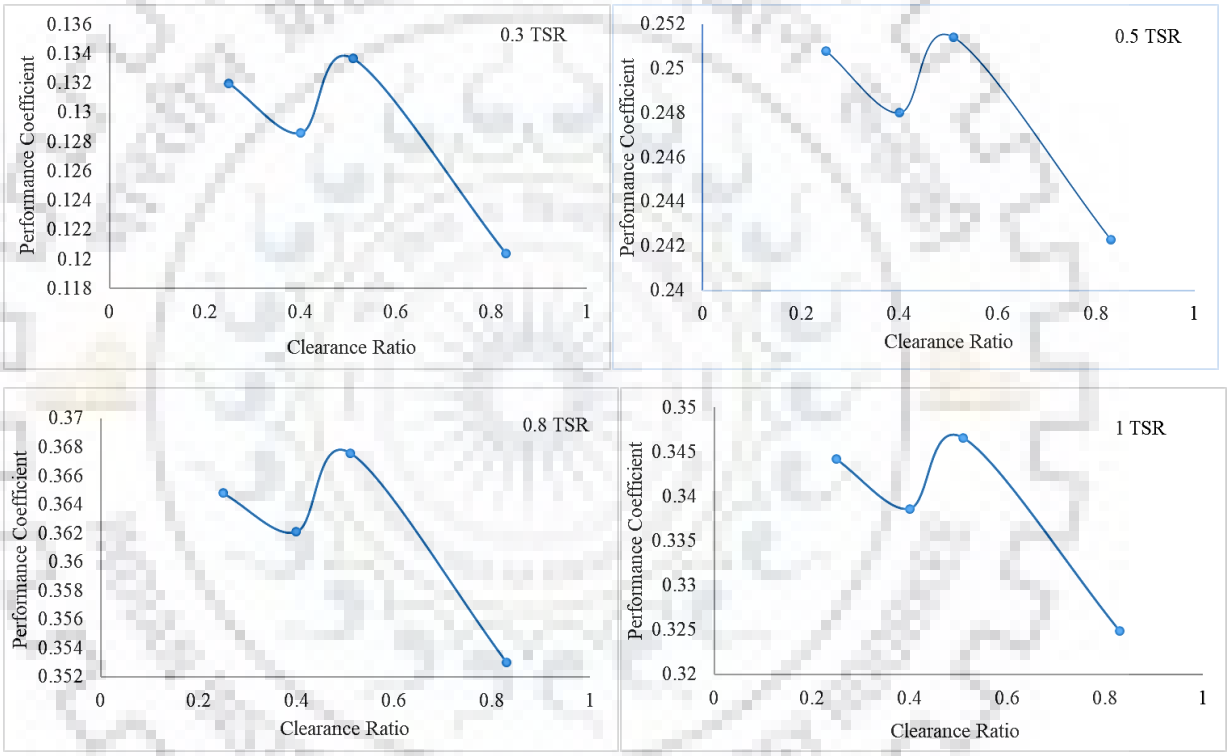

Fig 4.11 Performance Coefficient Vs Clearance Ratio

4.6.2 Relationship between Performance Coefficient and Tip Speed Ratio

The relationship between coefficient of power and tip speed ratio is shown in Fig. 4.12. At a clearance ratio of 0.51 the coefficient of performance is maximum at all values of tip speed ratio. For the tip speed ratio of 0.8 maximum power coefficient is obtained for all the cases of clearance ratios but after 0.8 TSR the curve drops and attains a lower power coefficient equal to 0.3466 at a TSR of 1.0 and further it follows the same trend. Therefore, it was found that a maximum power coefficient of 0.3466 is obtained at a TSR of 0.8 for a clearance ratio of 0.51.

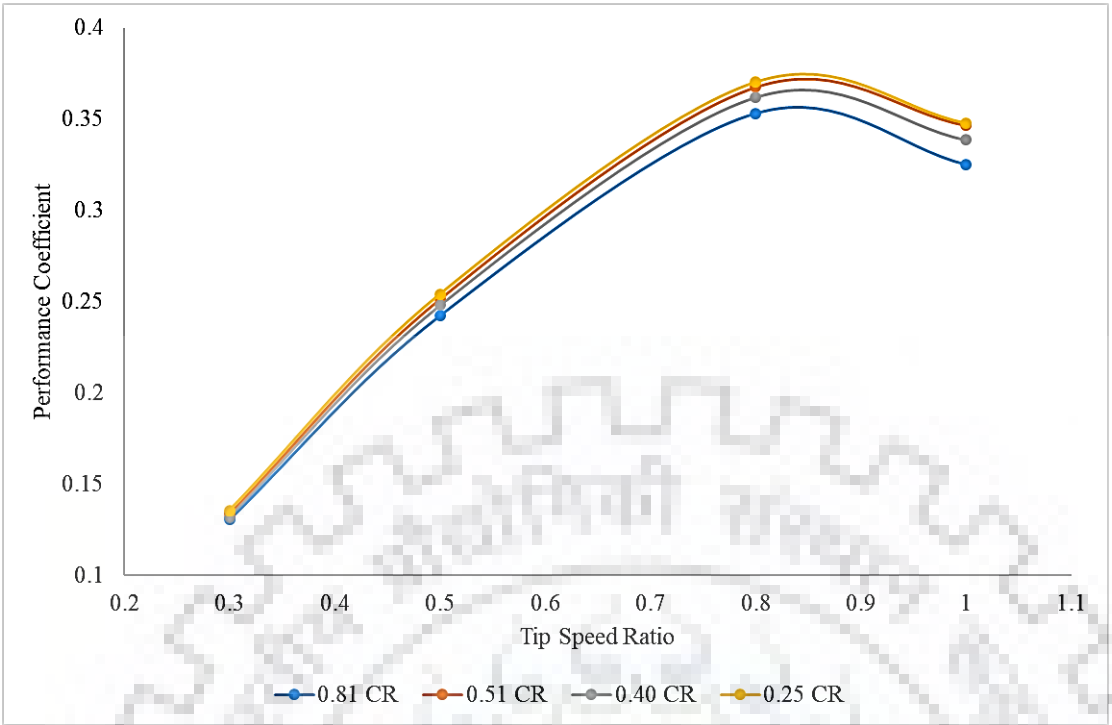

Fig. 4.12 Performance Coefficient Vs Tip Speed Ratio at different Clearance Ratios

The value of performance coefficient increases up to a tip speed ratio of 0.8 and then it starts decreasing. If the rotor blades rotates too slowly, blades will be unable capture most of the water and relatively less quantity of water will interact with the rotor. However, if the rotor blades are rotating at high RPM, then water will always flow in turbulent condition. There must be adequate time lapses between two blades moving through the same location so that nearby water can move in and power can be harnessed from it.

4.6.3 Relationship between Coefficient of Torque and Tip Speed Ratio

The next important parameter is the torque coefficient. The value of torque coefficient increases from 0.3 TSR to 0.5 TSR then the value of the torque coeffcient decreases unlike the power coefficient which decreases after 0.8 TSR. In the present the value of torque coefficient has maximum value of 0.5028 at 0.5 TSR at a clearance ratio of 0.51. The variation of torque coefficient with TSR at different clearance ratio is shown in Fig. 4.13.

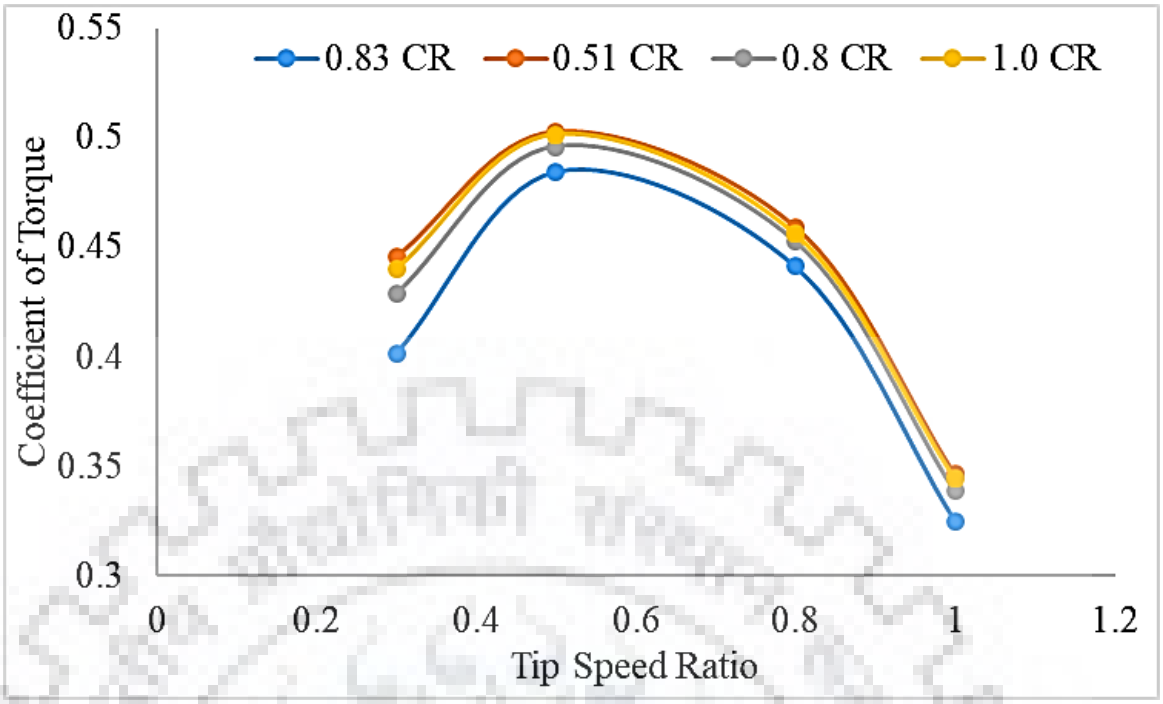

Fig. 4.13 Coefficient of Torque Vs Tip Speed Ratio at different Clearance Ratio

4.6.4 Comparison of the previous experimental study with present numerical investigation

The d/D is the clearance ratio which varies from 0.10 to 1.08 for the experimental work done by Nakajima et al. [51]. Fig 4.14 shows a comparison between the previous experimental work done and the present study.

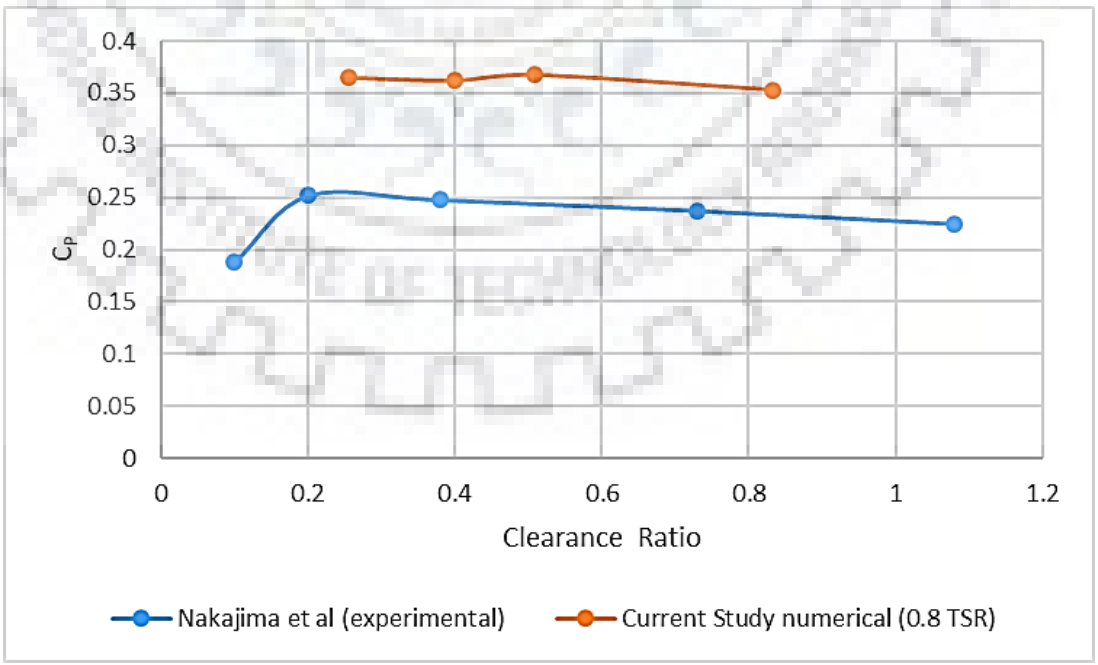

Fig 4.14 Comparison of Performance Coefficient vs Clearance Ratio

As seen from the graph the curve exhibits maximum performance coefficient for clearance ratio of 0.20. The performance coefficient decreased with increasing the clearance coefficient. The reason seems to be the stagnation flow along the convex side of the returning blade which increases the fluid as the rotor is close to the water surface.

In current study the graph is similar to the experimental study performed be Nakajima et al. The maximum value of the performance coefficient is 0.3676 at 0.51 clearance ratio. It was observed that the effect of turbulence is maximum in the proximity of the channel bottom therefore the performance coefficient decreases slightly and then increases.

CHAPTER 5

CONCLUSIONS AND RECOMMENDATIONS

5.1 CONCLUSIONS

Under the present dissertation work, the site parameters of hydrokinetic turbine are identified. The effect of identified site parameters are analyzed through various literature studies and it has been found that the installation of hydrokinetic turbine plays a pivotal role for the optimum utilization of site potential. Based on the literature review, clearance ratio is selected as the installation parameter and CFD based numerical simulations analysis was carried out on the 3D model of Savonius hydrokinetic turbine along with the channel resembling the actual site conditions. The clearance ratio was varied by changing the depth of installation. Based on the present study following conclusions may be drawn:

i. Placement of the hydrokinetic turbine is governed by the clearance ratio and it depends on the vertical velocity gradient and turbulence intensity of the flow.
ii. Savonius rotor hydrokinetic turbine yields its maximum performance corresponding to clearance ratio of 0.51 and 1.5 m/s and 0.8 value of flow velocity and TSR respectively.
iii. In order to validate the CFD results an attempt has also been made to compare the numerical results obtained under present study with the previous experimental work and it has been found that numerical results are consistent and follow the similar trends. The value of C_P is found to be minimum at maximum clearance ratio (d/D).
iv. Further, the effect of blockage ratio at low operating range (TSR) is found to be negligible. For high operating conditions (high TSR), a significant change in performance was observed.

5.2 RECOMMENDATIONS

Based on the CFD analysis, it is found that further studies are required to carry out the in depth investigation on the following areas of Savonius hydrokinetic turbine;

i. There is need to test the CFD analysis of the turbine under the actual site conditions.
ii. The future scope may be directed towards the performance comparison of different hydrokinetic turbines at different installation depths of the channel.
iii. The techno-economic analysis of these technologies need to be carried out.

REFERENCES

[1] https://www.worldenergy.org/wp-content/uploads/2016/10/World-Energy-Scenarios-2016_Full-Report.pdf.

[2] Central Electricity Authority, "All India Installed Capacity of Power Stations," Minist. Power, Gov. India, vol. I, no. 5, pp. 1–7, 2016.

[3] A. Sinha and M. Shahbaz, "Estimation of Environmental Kuznets Curve for CO2emission: Role of renewable energy generation in India," Renew. Energy, vol. 119, pp. 703–711, 2018.

[4] S. Sen, S. Ganguly, A. Das, J. Sen, and S. Dey, "Renewable energy scenario in India: Opportunities and challenges," J. African Earth Sci., vol. 122, pp. 25–31, 2016.

[5] Indian Renewable Energy Development Agency Limited (IREDA) Study on Tidal & Waves Energy in India : Survey on the Potential & Proposition of a Roadmap," no. December, 2014.

[6] L. Tripathi, A. K. Mishra, A. K. Dubey, C. B. Tripathi, and P. Baredar, "Renewable energy: An overview on its contribution in current energy scenario of India," Renew. Sustain. Energy Rev., vol. 60, pp. 226–233, 2016.

[7] http://eagri.org/eagri50/AENG352/lec26.pdf.

[8] M. J. Khan, G. Bhuyan, M. T. Iqbal, and J. E. Quaicoe, "Hydrokinetic energy conversion systems and assessment of horizontal and vertical axis turbines for river and tidal applications: A technology status review," Appl. Energy, vol. 86, no. 10, pp. 1823–1835, 2009.

[9] M. J. Khan, M. T. Iqbal, and J. E. Quaicoe, "River current energy conversion systems: Progress, prospects and challenges," Renew. Sustain. Energy Rev., vol. 12, no. 8, pp. 2177–2193, 2008.

[10] M.-H. Briand and K. Ng, "Kinetic Energy Recovery Turbine Technology : Resource Assessment and Site Development Strategy," World Energy Conf. Energy Resour. Technol. today tomorrow, no. 2.1, pp. 1–12, 2010.

[11] M. Anyi and B. Kirke, "Tests on a non-clogging hydrokinetic turbine," Energy Sustain. Dev., vol. 25, pp. 50–55, 2015.

[12] R. Noruzi, M. Vahidzadeh, and A. Riasi, "Design, analysis and predicting hydrokinetic performance of a horizontal marine current axial turbine by consideration of turbine installation depth," Ocean Eng., vol. 108, pp. 789–798, 2015.

[13] J. Riglin, C. Daskiran, J. Jonas, W. C. Schleicher, and A. Oztekin, "Hydrokinetic turbine array characteristics for river applications and spatially restricted flows," Renew. Energy, vol. 97, pp. 274–283, 2016.

[14] S. Chawdhary et al., “Wake characteristics of a TriFrame of axial-flow hydrokinetic turbines,” Renew. Energy, vol. 109, pp. 332–345, 2017.

[15] Z. Hu and X. Du, “Reliability analysis for hydrokinetic turbine blades,” Renew. Energy, vol. 48, pp. 251–262, 2012.

[16] J. Riglin, W. Chris Schleicher, I. H. Liu, and A. Oztekin, “Characterization of a micro-hydrokinetic turbine in close proximity to the free surface,” Ocean Eng., vol. 110, pp. 270–280, 2015.

[17] M. S. Guney, “Evaluation and measures to increase performance coefficient of hydrokinetic turbines,” Renew. Sustain. Energy Rev., vol. 15, no. 8, pp. 3669–3675, 2011.

[18] T. Kinsey and G. Dumas, “Impact of channel blockage on the performance of axial and cross-flow hydrokinetic turbines,” Renew. Energy, vol. 103, pp. 239–254, 2017.

[19] C. Hill, M. Musa, and M. Guala, “Interaction between instream axial flow hydrokinetic turbines and uni-directional flow bedforms,” Renew. Energy, vol. 86, pp. 409–421, 2016.

[20] A. T. D. Déborah, R. Vaz, J. R. P. Vaz, and P. A. S. F. Silva, “Energy for Sustainable Development An approach for the optimization of diffuser-augmented hydrokinetic blades free of cavitation,” Energy Sustain. Dev., vol. 45, pp. 142–149, 2018.

[21] W. Wang, R. Yin, and Y. Yan, “horizontal axis micro-hydrokinetic river turbine,” Renew. Energy, 2018.

[22] P. Aghsaee and C. D. Markfort, “Effects of fl ow depth variations on the wake recovery behind a horizontal-axis hydrokinetic in-stream turbine,” Renew. Energy, vol. 125, pp. 620–629, 2018.

[23] N. Kolekar and A. Banerjee, “Performance characterization and placement of a marine hydrokinetic turbine in a tidal channel under boundary proximity and blockage effects,” Appl. Energy, vol. 148, pp. 121–133, 2015.

[24] P. Pyakurel, J. H. VanZwieten, C. Sultan, M. Dhanak, and N. I. Xiros, “Numerical simulation and dynamical response of a moored hydrokinetic turbine operating in the wake of an upstream turbine for control design,” Renew. Energy, vol. 114, pp. 1134–1145, 2017.

[25] U. Tewari, D. Norta, and K. Kolmsee, “Hydrokinetic Energy for Enlightening the,” Ichpsd, pp. 146–157, 2015.

[26] P. K. Talukdar, V. Kulkarni, and U. K. Saha, “Field-testing of model helical-bladed hydrokinetic turbines for small-scale power generation,” Renew. Energy, vol. 127, pp. 158–167, 2018.

[27] A. H. Birjandi, E. L. Bibeau, V. Chatoorgoon, and A. Kumar, “Power measurement of hydrokinetic turbines with free-surface and blockage effect,” Ocean Eng., vol. 69, pp. 9–17, 2013.

[28] A. C. Fernandes and A. Bakhshandeh Rostami, “Hydrokinetic energy harvesting by an innovative vertical axis current turbine,” Renew. Energy, vol. 81, pp. 694–706, 2015.

[29] A. Kumar and R. P. Saini, “Performance analysis of a single stage modi fi ed Savonius hydrokinetic turbine having twisted blades,” Renew. Energy, vol. 113, pp. 461–478, 2017.

[30] N. K. Sarma, A. Biswas, and R. D. Misra, “Experimental and computational evaluation of Savonius hydrokinetic turbine for low velocity condition with comparison to Savonius wind turbine at the same input power,” Energy Convers. Manag., vol. 83, pp. 88–98, 2014.

[31] B. K. Kirke, “Tests on ducted and bare helical and straight blade Darrieus hydrokinetic turbines,” Renew. Energy, vol. 36, no. 11, pp. 3013–3022, 2011.

[32] S. Sharma and R. K. Sharma, “Performance improvement of Savonius rotor using multiple quarter blades – A CFD investigation,” Energy Convers. Manag., vol. 127, pp. 43–54, 2016.

[33] D. Forbush, B. Polagye, J. Thomson, L. Kilcher, J. Donegan, and J. McEntee, “Performance characterization of a cross-flow hydrokinetic turbine in sheared inflow,” Int. J. Mar. Energy, vol. 16, pp. 150–161, 2016.

[34] P. K. Talukdar, A. Sardar, V. Kulkarni, and U. K. Saha, “Parametric analysis of model Savonius hydrokinetic turbines through experimental and computational investigations,” Energy Convers. Manag., vol. 158, no. January, pp. 36–49, 2018.

[35] L. I. Lago, F. L. Ponta, and L. Chen, “Advances and trends in hydrokinetic turbine systems,” Energy Sustain. Dev., vol. 14, no. 4, pp. 287–296, 2010.

[36] J. Petrie, P. Diplas, M. Gutierrez, and S. Nam, “Characterizing the mean flow field in rivers for resource and environmental impact assessments of hydrokinetic energy generation sites,” Renew. Energy, vol. 69, pp. 393–401, 2014.

[37] M. Anyi and B. Kirke, “Evaluation of small axial flow hydrokinetic turbines for remote communities,” Energy Sustain. Dev., vol. 14, no. 2, pp. 110–116, 2010.

[38] L. L. Ladokun, B. F. Sule, K. R. Ajao, and A. G. Adeogun, “Resource assessment and feasibility study for the generation of hydrokinetic power in the tailwaters of selected hydropower stations in Nigeria,” Water Sci., no. 2017, 2018.

[39] V. S. Neary, B. Gunawan, and D. C. Sale, “Turbulent inflow characteristics for hydrokinetic energy conversion in rivers,” Renew. Sustain. Energy Rev., vol. 26, pp. 437–445, 2013.

[40] A. H. Birjandi, S. D’Auteuil, C. Ridd, and E. L. Bibeau, “An innovative low cost hydrokinetic site selection technique for cold climate regions,” MTS/IEEE Ocean. 2015 - Genova Discov. Sustain. Ocean Energy a New World, pp. 1–4, 2015.

[41] K. Kusakana and H. J. Vermaak, “Hydrokinetic power generation for rural electricity supply: Case of South Africa,” Renew. Energy, vol. 55, pp. 467–473, 2013.

[42] T. Kinsey et al., “Prototype testing of a hydrokinetic turbine based on oscillating hydrofoils,” Renew. Energy, vol. 36, no. 6, pp. 1710–1718, 2011.

[43] M. R. Motley and R. B. Barber, “Passive control of marine hydrokinetic turbine blades,”

Compos. Struct., vol. 110, no. 1, pp. 133–139, 2014.

[44] E. González-Gorbeña, R. Y. Qassim, and P. C. C. Rosman, “Optimisation of hydrokinetic turbine array layouts via surrogate modelling,” Renew. Energy, vol. 93, pp. 45–57, 2016.

[45] J. Lata-García, F. Jurado, L. M. Fernández-Ramírez, and H. Sánchez-Sainz, “Optimal hydrokinetic turbine location and techno-economic analysis of a hybrid system based on photovoltaic/hydrokinetic/hydrogen/battery,” Energy, vol. 159, pp. 611–620, 2018.

[46] B. Gunawan, M. Richmond, and V. Durgesh, Field Measurements at River and Tidal Current Sites for Hydrokinetic Energy Development: Best Practices Manual, no. September. 2011.

[47] J. Goundar and M. R. Ahmed, “Design and Optimization of a Horizontal Axis Marine Current Turbine.”

[48] J. M. R. Gorle, L. Chatellier, F. Pons, and M. Ba, “Flow and performance analysis of H-Darrieus hydroturbine in a confined flow: A computational and experimental study,” J. Fluids Struct., vol. 66, pp. 382–402, 2016.

[49] M. A. Kamoji, S. B. Kedare, and S. V Prabhu, “Experimental investigations on single stage modified Savonius rotor,” vol. 86, pp. 1064–1073, 2009.

[50] V. Patel, T. I. Eldho, and S. V Prabhu, “Velocity and performance correction methodology for hydrokinetic turbines experimented with different geometry of the channel,” Renew. Energy, pp. 1–18, 2018.

[51] M. Nakajima, S. Iio, and T. Ikeda, “Performance of Savonius Rotor for Environmentally Friendly Hydraulic Turbine,” J. Fluid Sci. Technol., vol. 3, no. 3, pp. 420–429, 2008.